HHS Public Access

Author manuscript

Neuron. Author manuscript; available in PMC 2020 December 04.

Published in final edited form as:

Neuron. 2019 December 04; 104(5): 916–930.e5. doi:10.1016/j.neuron.2019.10.032.

Complementary Genetic Targeting and Monosynaptic Input Mapping Reveal Recruitment and Refinement of Distributed Corticostriatal Ensembles by Cocaine

Nicholas R. Wall[1,4], **Peter A. Neumann**[1,4], **Kevin T. Beier**[1,2,3], **Ava K. Mokhtari**[1], **Liqun Luo**[2], **Robert C. Malenka**[1,5,*]

[1]Nancy Pritzker Laboratory, Dept. of Psychiatry & Behavioral Sciences

[2]Dept. of Biology, Howard Hughes Medical Institute, Stanford University School of Medicine, Stanford, CA. 94305, USA

[3]Present address: Dept. of Physiology & Biophysics, University of California, Irvine, Irvine, CA 92697, USA

[4]These authors contributed equally

[5]Lead Contact

SUMMARY

Drugs of abuse elicit powerful experiences that engage populations of neurons broadly distributed throughout the brain. To determine how synaptic connectivity is organized to enable robust communication between populations of drug-activated neurons, we developed a complementary targeting system for monosynaptic rabies virus (RV) tracing that identifies direct inputs to activated versus non-activated neuronal populations. Analysis of over 100,000 synaptic input neurons demonstrated that cocaine-activated neurons comprise selectively connected, but broadly distributed, corticostriatal networks. Electrophysiological assays using optogenetics to stimulate activated versus non-activated inputs revealed stronger synapses between co-activated cortical pyramidal neurons and neurons in the dorsal striatum (DS). Repeated cocaine exposure further enhanced the connectivity specifically between drug-activated neurons in the orbitofrontal cortex (OFC) and co-active DS neurons. Selective chemogenetic silencing of cocaine-activated OFC neurons or their terminals in DS disrupted behavioral sensitization, demonstrating the utility of this methodology for identifying novel circuit elements that contribute to behavioral plasticity.

*Correspondence: malenka@stanford.edu.

AUTHOR CONTRIBUTIONS

N.R.W., P.A.N., and R.C.M. conceived experiments, wrote the manuscript, and secured funding. N.R.W., P.A.N., and A.K.M. performed experiments. K.T.B. provided reagents and technical expertise. L.L. and R.C.M. provided expertise and feedback. All authors edited the manuscript.

DECLARATION OF INTERESTS

The authors declare no competing interests.

INTRODUCTION

Due to recent methodological advances, investigators are now able to use intersectional genetic strategies to observe and manipulate specific cell types based on their molecular phenotype and projection targets, leading to advances in our understanding of the neural circuit basis of behavior (Luo et al., 2008, 2018). A particularly important advance has been the development of methods that allow genetic access to the ensembles of neurons activated by a specific experience, and which presumably play a critical role in the behavioral plasticity. Typically, these methods use activation of immediate early genes (IEGs) to identify and capture the activated neurons for subsequent analysis and manipulation (Luo et al., 2018). Approaches include expression of recombinases under the control of IEG promoters in transgenic/knockin mice (i.e. TRAP mouse lines) (DeNardo et al., 2019; Girasole et al., 2018; Guenthner et al., 2013; Ye et al., 2016), expression of other molecular switches in an IEG-dependent manner (Choi et al., 2018; Ramirez et al., 2013; Ryan et al., 2015), and viral-mediated expression of transgenes driven by IEG promoters (Choi et al., 2018; Zhang et al., 2015). Application of these methods has greatly advanced our understanding of, for example, engram formation (Josselyn and Frankland, 2018; Tonegawa et al., 2018) and circuits mediating primary motivational drives (Allen et al., 2017). Previous studies using IEG-based techniques to identify and silence the neuronal ensembles activated by cocaine and other psychostimulants found functionally important activated ensembles in several brain regions including the nucleus accumbens (NAc), medial prefrontal cortex, and DS (Caprioli et al., 2017; Cruz et al., 2013). Detailed analysis of the drug-activated neurons also revealed potentially important changes in their electrophysiological and molecular properties (Cruz et al., 2013; Li et al., 2015; Rubio et al., 2015; Whitaker et al., 2016).

A common limitation of IEG-based studies is that the activated neurons being studied are restricted to a single or small number of brain areas. Furthermore, the synaptic connectivity of the activated neuronal ensembles is often unknown, as is the behavioral relevance of such connectivity. Clearly, neurons do not function in isolation but are commonly driven to spike in response to the complex interplay of thousands of synaptic inputs. To address this topic, we combined several recently developed yet well-established methods: Cre-dependent monosynaptic RV tracing (Wall et al., 2010), TRAP mice (Guenthner et al., 2013), and Cre-ON and Cre-OFF viral mediated transgene expression (Beier et al., 2017; Saunders et al., 2012). By injecting Cre-dependent viruses that enable targeted RV infection and monosynaptic retrograde spread in complementary populations of neurons, we identified activated and non-activated cells sending monosynaptic inputs to activated or non-activated neuronal ensembles in the targeted structure. Finally, by using Cre-ON and Cre-OFF viruses expressing transgenes for optogenetic or chemogenetic manipulation of neuronal populations, we assayed the properties of synapses made between activated versus non-activated ensembles of neurons as well as the behavioral role of these ensembles. To test the utility of these methodologies in advancing our understanding of the neural circuit dynamics that contribute to behavioral plasticity, we examined a robust, well-established form of experience-dependent plasticity, cocaine-induced behavioral sensitization, which commonly is used as a surrogate for the drug-elicited craving that leads to relapse during addiction

(Robinson and Berridge, 2003; Valjent et al., 2010; Vanderschuren and Kalivas, 2000; Vezina, 2007; Wolf, 1998; Wolf and Ferrario, 2010).

We expand on prior studies by assaying the brain-wide synaptic connectivity of cocaine-activated ensembles, focusing on corticostriatal projection systems. We find differences in the properties of synapses between activated and non-activated neuronal ensembles and, as a consequence of repeated cocaine administration, behaviorally relevant changes in the pattern of connectivity of activated ensembles. These findings validate the utility of the novel approaches we have taken and suggest that these strategies can assist in elucidating the complex changes in neural circuits that mediate experience-dependent behavioral plasticity.

RESULTS

Cocaine-activated Neurons in DS and Cortex

To gain genetic access to populations of neurons activated by a cocaine experience, we utilized a line of mice that expresses CreER^{T2} under the control of the *Arc* promoter: Arc-TRAP (Guenthner et al., 2013), which is upregulated by neuronal activity (Bramham et al., 2010). When 4-hydroxytamoxifen (4-OHT) is provided in conjunction with a stimulus, Cre-mediated recombination is enabled specifically in neurons that were activated during the stimulus period (Guenthner et al., 2013; Ye et al., 2016). Arc-TRAP animals were crossed with Ai14 reporter mice (Madisen et al., 2010), which express Cre-dependent tdTomato, labeling activated cells red (Arc-TRAP/Ai14, Figure S1A).

To capture neuronal populations activated by a strong drug experience, Arc-TRAP/Ai14 mice were administered 4-OHT paired with either cocaine or saline. Cocaine exposure increased the number of tdTomato-expressing neurons, notably in the DS (Figures S1B and S2), including both dorsomedial and dorsolateral striatal subregions (Figures S1C and S1D). Cocaine administration also increased the number of activated neurons broadly throughout cortex (Figures S1E–S1J). Much of the shared signal in saline and cocaine-treated animals occurs in layer 6 neurons (Figure S1F), which were previously characterized as exhibiting nonspecific activation in the absence of tamoxifen (Guenthner et al., 2013). To verify the activity dependence of tdTomato expression, selective sensory deprivation was performed in Arc-TRAP/Ai14 animals by plucking single whiskers (Figure S1K). Many fewer activated neurons were detected in the somatosensory whisker barrel associated with the excised whisker (Figures S1L–S1N).

Cocaine-Activated Corticostriatal Ensembles

To elucidate how drug-activated neurons are connected to form integrated, coherent neuronal ensembles, we applied monosynaptic rabies tracing in the DS of cocaine-exposed Arc-TRAP/Ai14 animals. Cre-ON or Cre-OFF adeno-associated viruses (AAVs) expressing the avian viral receptor TVA and rabies glycoprotein (RG) were co-injected into the DS of Arc-TRAP/Ai14 animals (Figures 1A and 1B). Cre-ON viruses enable the generation of monosynaptic connectivity maps of inputs to cocaine-activated neurons while Cre-OFF viruses enable input maps onto neurons not activated by cocaine (Figure 1C). As an additional control, we injected RV with native RG on its surface, which acts as a traditional

retrograde tracer that is taken up non-selectively at axon terminals near the injection site (Figure 1C), providing a means for assessing the overall organization of corticostriatal projections. Since non-activated neurons make up most of the total neurons, we expect that the data acquired using the Retrograde RV will more closely approximate the Cre-OFF condition. RV vectors expressing green fluorescent protein (GFP) were injected three weeks following cocaine exposure and allowed to express and spread for one week (Figure 1A). Robust tdTomato and GFP labeling was detectable (Figures 1D–1L) at both the DS injection site and throughout cortex, allowing identification of activated neurons (red) and rabies-labeled neurons (green). The area of DS directly infected with RV (Figure 1D–1F, bottom right) consists of GFP-labeled starter cells as well as local, monosynaptically connected neurons. GFP-labeled neurons in cortex (Figures 1G–1L) and other non-striatal brain regions are exclusively monosynaptically connected to the genetically targeted DS cell population.

A comprehensive description of the locations of total corticostriatal input in all three conditions is displayed both as a group summary (Figure 2A) and as individual animal data (Figure 2B). Reported values include inputs arising from both neocortical and periallocortical sources, but do not include neurons from other input structures such as the thalamus. Raw data for all conditions are provided in Supplemental Excel File 1. Cocaine-activated DS neurons (Figures 2A, 2B, yellow) received monosynaptic input from the same set of brain regions that provide input to non-activated neurons (Figures 2A, 2B, green), and to the targeted region of DS as a whole (Figures 2A, 2B, gray). We then identified brain regions that provided significantly different input in Cre-ON versus both Cre-OFF and Retrograde RV. There was a slight but significant increase in input arising from ventral OFC and from a portion of cingulate cortex targeting cocaine-activated neurons in the striatum. Individual variability (Figure 2B) combined with the low absolute magnitude of these changes makes it difficult to ascertain the biological significance of these findings in a vacuum, but these observations will provide useful supporting evidence when combined with data gathered in subsequent experiments (Figure 5).

To assess the degree to which drug-activated neurons preferentially wire onto one another, cortical rabies-labeled cells were quantified based on their concurrent Cre-dependent tdTomato expression. Neurons expressing both tdTomato and GFP were yellow and represented monosynaptically connected corticostriatal projection neurons activated by cocaine, whereas green neurons were not activated by the cocaine experience (Figure 3A). An index measuring the proportion of input arising from cocaine-activated cortical neurons in each cortical area (Figure 3B) was used to assess connectivity patterns across all three conditions (Figures 3C–3N). Across cortical areas, cocaine-activated corticostriatal neurons preferentially made connections onto cocaine-activated DS neurons (Figure 3O, yellow bars). Non-activated neurons in striatum received a lower proportion of cocaine-activated cortical input (Figure 3O, green bars). Importantly, as hypothesized earlier, the proportion of activated cortical neurons sending projections to striatum using retrograde RV (Figure 3O, grey hatched bars) was similar to that obtained when examining activated cortical neurons making synapses onto non-activated DS neurons. Input differences were apparent at the individual animal level (Figure 3P), indicating a robust and reliable enhancement of connectivity from cocaine-activated neurons across many input regions. These results suggest that neurons activated by cocaine and presumably dedicated to processing drug-

specific information form preferentially connected corticostriatal networks involving virtually all areas of cortex.

One explanation for the preferential connectivity between drug-activated cortical and drug-activated DS neurons is that the cocaine-activated corticostriatal neurons simply drive more activity in their downstream striatal partners, making these cells more likely to be labeled with tdTomato following drug exposure. If this explanation accounts for our results, we would expect any populations of neurons activated by a common experience to show this same preferential connectivity. To assess this possibility, we assayed the monosynaptic inputs to DS neurons activated by a saline injection combined with the animal's normal home cage experience. Saline-activated cortical neurons did not show enhanced levels of connectivity to saline-activated DS neurons when compared to the connectivity of populations of neurons activated by a cocaine/home cage experience (Figure S3). This difference suggests that the enhanced corticostriatal connectivity generated by cocaine administration was unique to the cocaine experience and is not simply a property of any pre-existing, strongly connected corticostriatal ensemble.

Properties of Corticostriatal Synapses in Activated Versus Non-activated Neuronal Ensembles

To assess the properties of corticostriatal synapses between sets of cocaine-activated and non-activated cortical and DS neurons, we injected AAVs expressing either Cre-ON or Cre-OFF ChR2-eYFP into the motor cortex of Arc-TRAP/Ai14 animals (Figures 4A–4C), followed by a single cocaine exposure paired with 4-OHT (Figure 4D). Three weeks after drug injections, we performed whole-cell voltage-clamp recordings either from cocaine-activated (Figure 4D, red) or non-activated neurons in the DS (Figure 4D, gray) while optically stimulating corticostriatal terminals originating from either cocaine-activated (Figure 4D, yellow) or non-activated (Figure 4D, green) cortical neurons. We also simultaneously activated unidentified striatal inputs via interleaved electrical stimulation (Figure 4D). We attempted to restrict our recordings to medium spiny neurons (MSNs) based on electrophysiological characteristics (see STAR*Methods), but future references to MSNs should be considered "putative MSNs" since neuronal identity was not biochemically characterized post-hoc.

Paired-pulse ratios (PPRs) of AMPA receptor-mediated excitatory postsynaptic events (AMPAR EPSCs), which inversely correlate with the probability of transmitter release (Zucker and Regehr, 2002), were smaller at active to active (A→A) synapses than at all other synapse types (Figures 4E and 4F). Furthermore, PPRs generated by stimulation of non-activated cortical inputs onto activated DS MSNs (N^-A) were smaller than those recorded from non-activated MSNs (N→N), as were the PPRs generated by electrical stimulation (E→A < E→N) (Figures 4G and 4H). These findings suggest that synapses made by cocaine-activated cortical neurons onto cocaine-activated DS MSNs have a higher probability of release than synapses made between all other cell combinations.

As a global measure of postsynaptic properties at these excitatory connections, we assessed the ratio of AMPAR EPSCs to NMDAR EPSCs. AMPAR/NMDAR ratios were enhanced at A→A synapses when compared with A→N and N→N synapses (Figures 4I and 4J).

AMPAR/NMDAR ratios generated by electrical stimulation were not different between activated and non-activated DS MSNs (Figures 4K and 4L), presumably because excitatory inputs from a wide range of brain areas were stimulated indiscriminately.

To determine if increased AMPAR/NMDAR ratio at A→A synapses involves enhanced AMPAR-mediated signaling, we optogenetically stimulated corticostriatal terminals arising from cocaine-activated neurons and measured the amplitude of strontium-mediated asynchronous release events (Oliet et al., 1996). Average miniature event amplitude was increased at A→A synapses compared to the A→N synapses, indicating enhanced AMPAR-mediated transmission in the cocaine-activated corticostriatal circuit (Figures 4M and 4N). Taken together, these electrophysiological results suggest that synapses between cocaine-activated upstream cortical neurons and downstream DS neurons possess both postsynaptic increases in AMPAR-mediated transmission and presynaptic enhancements of transmitter release.

Chronic Administration Shifts Cocaine-activated Corticostriatal Ensembles

The development of addiction requires neural adaptations caused by repetitive drug use. To determine if the corticostriatal ensembles activated by cocaine change with repeated administration, we applied monosynaptic RV tracing in mice that had previously received 7 days of saline or cocaine, which is known to cause robust behavioral sensitization lasting several weeks (Robinson and Berridge, 2003; Vezina, 2007; Wolf, 1998). Following chronic cocaine or saline administration, Cre-ON AAVs coding for TVA and RG were injected into the DS of Arc-TRAP/Ai14 mice, and mice were subsequently administered a single cocaine injection paired with 4-OHT (Figure 5A). RV injection 3 weeks later (Figure 5A) labeled inputs onto cocaine-activated DS neurons (Figures 5B–5E), with any differences between the saline and cocaine treated animals reflecting long-term changes in connectivity due to the prior chronic cocaine exposure that occurred six weeks before.

Following repeated cocaine exposure, overall inputs arose from the same set of cortical areas across conditions (Figure S4). Activated cortical neurons across brain regions retained their tight coupling with co-active DS neurons, maintaining or exceeding proportions of activated inputs to those observed with no prior cocaine exposure (Figure 5F, 5G). Chronic cocaine caused a significant increase in the proportion of cocaine-activated neurons in the OFC synapsing on cocaine-activated DS neurons (Figure 5F, 5G). The most dramatic increases in coupling between co-active neurons were observed in the lateral OFC (Figure 5H), with average co-connectivity nearing 50%, but ventral OFC also showed enhanced connectivity. Following chronic cocaine administration, cocaine-activated neurons in both superficial and deep layers of OFC showed enhanced connectivity with activated DS neurons (Figure 5I). Furthermore, similar to the properties of the synapses between cocaine-activated motor cortex neurons and activated DS MSNs, synapses between cocaine-activated OFC neurons and activated DS MSNs (Figures 5J–5L) were stronger than those onto non-activated DS MSNs, as evidenced by smaller PPRs (Figures 5M and 5N) and increased AMPAR/NMDAR ratios (Figures 5O and 5P). Electrical stimulation revealed no differences between synapses onto activated versus non-activated DS MSNs (Figures 5M–5P). Combined with our previous observation of a larger proportion of total input arising from ventral OFC onto

acute cocaine-activated neurons versus non-activated neurons (Figure 2), these data suggest that OFC may be a critical region for mediating the consequences of repeated cocaine administration.

Inhibition of Activated OFC Inputs to Striatum Impairs Locomotor Sensitization

To determine whether the enhanced connectivity between activated OFC neurons and activated DS neurons due to chronic cocaine administration plays a role in mediating behavioral plasticity, we performed a locomotor sensitization assay and chemogenetically inhibited either cocaine-activated OFC neurons or non-activated OFC neurons using Cre-ON or Cre-OFF expression of the inhibitory DREADD hM4Di (Figure 6A). In animals expressing hM4Di in cocaine-activated neurons, expression of locomotor sensitization was significantly reduced when injected with CNO, whereas locomotor sensitization was unaffected in animals expressing hM4Di in non-activated OFC neurons (Figure 6B). Administration of CNO alone, in the absence of cocaine, did not decrease locomotion when compared to saline-injected animals (Figure 6C), ruling out the possibility that the generation of clozapine from CNO may have caused the CNO-mediated decrease in sensitized locomotor responses (Gomez et al., 2017) . These results demonstrate a specific role for cocaine-activated OFC neurons in the expression of locomotor sensitization.

To examine if cocaine-activated OFC neurons regulate behavioral sensitization specifically via their projections to the DS, we bilaterally injected Cre-dependent AAVs expressing hM4Di into OFC and implanted drug injection cannulae directly into the DS (Figure 6D). On the fourth day of cocaine exposure, animals received bilateral local infusions of CNO (300 μM, 300 nl) into the DS 30 minutes prior to behavioral assessment. Similar to the effects of systemic CNO administration, local inhibition of cocaine-activated OFC axon terminals in the DS reduced the expression of behavioral sensitization when compared to inhibition of non-activated axons. (Figure 6E). Again, CNO infusion in the absence of cocaine did not significantly affect locomotor activity in either the Cre-ON or Cre-OFF cohorts (Figure 6F). These data suggest that a relatively small population of cocaine-activated neurons in OFC plays a key role in regulating a prominent cocaine-mediated behavior via their projections to the DS and that these neurons can be functionally dissociated from the remainder of the orbitofrontal corticostriatal projection based on their IEG expression.

Locomotor Ensembles Do Not Show Persistent Enhancement of Connectivity

Cocaine has potent effects on locomotion as well as important non-locomotor effects. Although inactivation of cocaine activated cells in the OFC or their terminals in the DS did not impact basal locomotion (Figures 6C, 6F), it is conceivable that the cocaine-activated corticostriatal ensembles solely reflect the enhanced locomotion caused by cocaine and have little to do with its reinforcing or addicting properties. To address this issue, we captured neuronal populations activated by locomotion, independent of cocaine, by providing mice with wireless running wheels in their home cages (Figures 7A, 7B). This procedure allowed the mapping of monosynaptic inputs to DS neurons activated by locomotion (Figures 7C, 7E, and S5), compared to monosynaptic inputs to DS neurons activated by cocaine (Figures 7C, 7D, and S5). To ensure the mice exposed to running wheels increased their locomotion

at least as much as that induced by cocaine, we calculated the total distance traveled over the 90 minutes following a single dose of cocaine. On average, mice administered cocaine ran ~200 meters more than animals injected with saline (Figure 7F). This total distance was used as a minimum threshold to select mice based on their running wheel utilization (Figure 7G).

Connectivity between locomotor-activated corticostriatal input neurons and locomotor-activated DS neurons was markedly lower than the connectivity between the corticostriatal input neurons and DS neurons that were activated by cocaine (Figures 7H, 7I). To determine if the synapses between locomotor-activated corticostriatal neurons and locomotor-activated DS neurons possessed distinguishing characteristics, we injected AAVs expressing Cre-ON ChR2 into OFC (Figures 7J, 7K), and then made electrophysiological recordings from either locomotor-activated cells or non-activated cells in striatum while optogenetically stimulating locomotor-activated corticostriatal axon terminals (Figure 7L). In contrast to the differences in paired-pulse ratio and AMPAR/NMDAR ratio at corticostriatal synapses between cocaine-activated pairs of neurons (Figures 4, 5J–5P), no differences were detected at synapses between locomotor activated OFC neurons and activated DS neurons (Figures 7M–7P). Combined with our anatomical observations, these data suggest that neurons activated by increased locomotion do not maintain anatomically and physiologically distinct connection patterns, indicating that the persistent enhancement of connectivity we observed in cocaine-activated corticostriatal ensembles is likely due to non-locomotor processes impacted by cocaine.

Discussion

By combining several relatively new techniques in a novel manner, we have demonstrated that it is possible to identify and characterize novel, synaptically-connected neuronal ensembles that are required for behavioral plasticity. Specifically, by combining Arc-TRAP mice with complementary monosynaptic rabies virus tracing, we identified a previously unappreciated yet functionally important circuit component of the global brain network recruited by cocaine. Several novel findings emerged from this study. We found that populations of cocaine-activated neurons, distributed throughout cortex, selectively connected with co-activated neurons in the DS, forming a brain-spanning, monosynaptically connected ensemble. We demonstrated that this enhanced connectivity did not arise from the inherent activity of captured neurons, nor did this connectivity emerge as a secondary consequence of cocaine’s locomotor activating properties. When capturing populations of neurons activated by a single strong cocaine experience, we also found that repeated prior cocaine exposure resulted in further enhancement of connectivity between activated populations in OFC and DS. Importantly, the enhanced connectivity patterns we observed in our anatomical and physiological experiments persisted at least 3-4 weeks following a single strong cocaine exposure, and up to 6 weeks following chronic cocaine challenge. At least one prior study detected behavioral effects persisting up to 8 weeks following a single cocaine exposure (Valjent et al., 2010), hinting that cocaine-activated ensembles may retain their specialized connectivity for even longer than was documented in our experiments. These results add to the growing body of evidence demonstrating the advantages, and perhaps necessity, of capturing neuronal populations activated by individual stimuli to

precisely define neural circuit modifications mediating any form of experience-dependent plasticity (Cruz et al., 2015; Josselyn and Frankland, 2018; Tonegawa et al., 2018).

Synaptically connected cortical and DS neurons activated by a cocaine experience appear to have stronger synapses than the synapses between non-cocaine activated neurons. This enhanced synaptic strength is due to both stronger postsynaptic AMPAR-mediated responses and enhanced presynaptic probability of transmitter release. These differences also appear to be input-specific in that non-specific electrical activation of striatal inputs did not reveal major differences in the properties of synapses on cocaine-activated versus non-activated DS neurons. We cannot definitively state whether the stronger synapses were in fact generated by the cocaine experience or rather existed prior to drug administration. However, the magnitude of the paired-pulse ratios and AMPAR/NMDAR ratios at synapses between locomotor-activated OFC and DS neurons (Figures 7M–7P) suggest that these synapses are weaker than those between cocaine-activated OFC and DS neurons (Figures 5M–P). Such differences are most easily explained by the experiences themselves causing the observed changes in the measured synaptic properties.

We also showed that the specific connectivity between activated neuronal ensembles was required for the expression of locomotor sensitization. Surprisingly, inhibition of the larger proportion of non-cocaine activated OFC neurons had no effect on sensitization. While the medial prefrontal cortex has been heavily implicated in cocaine-mediated behavioral sensitization (Steketee, 2005), the role of the OFC has been controversial (Pierce et al., 1998; Schoenbaum et al., 2004; Valjent et al., 2010; Vanderschuren and Kalivas, 2000; Winstanley et al., 2009). The necessity of targeting the minority cocaine-activated OFC neuronal population to observe a clear behavioral effect may explain why previous work, which used coarser manipulations, produced inconsistent conclusions. It is important to note that while locomotor sensitization is a powerful exemplar of a cocaine-mediated behavior, future studies could build on our observations by explicitly exploring other aspects of the cocaine experience, such as its acute reinforcing effects and ability to influence the behavioral responses to specific cues and contexts.

The individual techniques we used are not without limitations. To date, it has been difficult to ascertain the physiological significance underlying monosynaptic RV labeling patterns. Recent work suggests that the efficiency of retrograde uptake and spread of RV is impacted by neuronal activity (Beier et al., 2017), identifying a potential substrate other than synapse number by which RV can spread. Furthermore, RV may exhibit tropism such that the detailed anatomy of the synapse influences the efficiency and extent of RV uptake (Albisetti et al., 2017; Wall et al., 2013). The ensemble targeting approach used here is agnostic regarding the absolute activity levels necessary to drive IEG promoter-mediated recombination in distinct neuronal types. In addition, transgene expression due to ectopic or spontaneous activation of the critical IEG degrades targeting precision and may reduce the statistical power of analyses derived using these populations. More recently developed mouse lines with increased expression fidelity (DeNardo et al., 2019) will be extremely valuable for future studies.

A decade ago, investigators first demonstrated that selective ablation of cocaine-activated NAc neurons, within a specific context, prevented subsequent context-specific locomotor sensitization (Koya et al., 2009). This important observation provided the motivation for subsequent studies, which demonstrated that IEG-expressing neuronal ensembles in several different brain regions, including NAc and DS, are required for learned behaviors related to several different classes of drugs of abuse (Cruz et al., 2013; Whitaker and Hope, 2018). Other changes in drug-activated neurons were also identified, including increases in intrinsic excitability (Ziminski et al., 2017) and in the proportion of putative silent synapses (Koya et al., 2012). We used our expanded genetic toolbox to demonstrate that monosynaptically connected drug-activated ensembles in fact span much of the brain, are linked with strengthened synapses to downstream partners in the DS, and that portions of these distributed ensembles regulate a prominent form of drug-induced behavioral plasticity. We anticipate that this combination of techniques will facilitate further exploration into the complex nature of neuronal ensembles activated by powerful experiences such as drugs of abuse, and may lead to the development of more sophisticated therapeutic strategies for reversing the pathological circuit adaptations underlying maladaptive behaviors.

STAR*METHODS

LEAD CONTACT AND MATERIALS AVAILABILITY

Further information and requests for resource and reagents should be directed to and will be fulfilled by the Lead Contact, Robert Malenka (malenka@stanford.edu). Plasmids generated in this study have been deposited to Addgene (pAAV-CAG-FLExOFF-TCB: Addgene 134980, pAAV-CAG-FLExOFF-RG: Addgene 134981). All unique/stable reagents generated in this study are available from the Lead Contact with a completed Materials Transfer Agreement.

EXPERIMENTAL MODEL AND SUBJECT DETAILS

All procedures were performed using standard protocols that conformed to NIH Guidelines for the Care and Use of Laboratory Animals and were approved by the Stanford University Administrative Panel on Laboratory Animal Care. Arc-TRAP (Jackson Laboratory B6.129(Cg)-Arctm1.1(cre/ERT2)Luo/J, Stock No: 021881) and Ai14 (Jackson Laboratory B6.Cg-Gt(ROSA)26Sortm14(CAG-tdTomato)Hze/J, Stock No: 007914) mice were maintained in a C57/B6J (JAX Stock No: 000664) background. Arc-TRAP mice were propagated in a heterozygous breeding population with C57/B6J breeding partners due to potential homozygous lethality. Arc/Ai14 experimental animals were produced through breeding homozygous positive Ai14 animals with heterozygous Arc-TRAP partners. Arc-TRAP positive offspring were determined via outsourced genotyping (Transnetyx, Inc.) with company standard Cre, ROSA26, and tdRFP primers. Animals across experimental groups were age, sex, and litter-matched as breeding permitted. Both male and female mice were used for all experiments.

METHOD DETAILS

Viral Vectors—AAV vectors were produced by the Stanford Viral Vector Core facility, with genomic titers determined by quantitative PCR. When possible, existing stock viruses

were used to enhance replicability and reproducibility. pAAV-CAG-FLEx-TCB ((Miyamichi et al., 2013), Addgene 48332) and pAAV-CAG-FLEx-RG ((Miyamichi et al., 2013), Addgene 48333) were used to produce Cre-ON AAV vectors (AAV2-CAG-FLEx-TCB titer $3x10^{12}$ GC/ml, AAV8-CAG-FLEx-RG titer $1x10^{12}$ GC/ml). pAAV-CAG-FLEx-OFF-TCB (Addgene 134980) was produced by PCRing the TCB cassette from pAAV-CAG-FLEx-TCB using primers containing SalI and AscI sites, and inserted into the same vector such that the fragment was inserted facing the forward direction. pAAV-CAG-FLEx-OFF-RG (Addgene 134981) was produced by PCRing the RG cassette from pAAV-CAG-FLEx-RG using primers containing SalI and AscI sites, and inserted into the same vector such that the fragment was inserted facing the forward direction (viral titers: AAV2-CAG-FLExOFF-TCB titer $1x10^{12}$ GC/ml, AAV8-CAG-FLExOFF-RG titer diluted to $1x10^{12}$ GC/ml using PBS on the viral injection day).

AAV-DJ-Cre-ON-ChR2(H134R)-eYFP was acquired from the Stanford Viral Vector Core (Stock virus GVVC-AAV-38). pAAV-CreOFF-ChR2(H134R)-eYFP was constructed by PCRing ChR2(H134R)-eYFP from pAAV-EF1a-DIO-ChR2(H134R)-eYFP (Addgene 20298) using primers containing SalI and AscI sites, and inserted into pAAV-hSyn-FLEx-mGFP-2A-Synaptophysin-mRuby (Beier et al., 2015) (Addgene 71760). The fragment was inserted facing in the forward direction such that Cre-mediated recombination inverts the ChR2(H134R)-eYFP cassette relative to the hSyn promoter. This plasmid was used to produce AAV-DJ-Cre-OFF-ChR2(H134R)-eYFP (titer $2x10^{14}$ GC/ml). AAV-DJ-Cre-ON-hm4Di-mCherry (Krashes et al., 2011) was acquired from the Stanford Viral Vector Core (Stock virus GVVC-AAV-129). pAAV-Cre-OFF-hM4Di-mCherry (also known as AAV-hsyn1-FLEx^{loxP}OFF-hM4Di-mCherry; (Beier et al., 2017)) was constructed by PCRing hM4Di-mCherry from pAAV-hSyn-DIO-hM4D(Gi)-mCherry (Addgene 44362) using primers containing SalI and AscI sites, and inserted into pAAV-hSyn-FLEx-mGFP-2A-Synaptophysin-mRuby (Addgene 71760). The fragment was inserted facing in the forward direction such that Cre-mediated recombination inverts the hM4Di-mCherry cassette relative to the hSyn promoter. This plasmid was used to produce AAV-DJ-Cre-OFF-hM4Di-mCherry (titer $1x10^{13}$ GC/ml). EnvA-pseudotyped RV vectors were produced from RVΔG-eGFP stocks as in (Wickersham et al., 2007). (EnvA)RVΔG-eGFP infectious titers were assessed through infection of TVA800-expressing HEK293T cells, with infectious titer of $1x10^{9}$ cfu/ml. Specificity to TVA-expressing cells was assessed through infection of HEK293T cells, verified $< 10^{4}$ cfu/ml in the absence of TVA.

In Vivo Stereotaxic Injections—Arc-TRAP/Ai14 or Arc-TRAP mice (40-50 days old) were prepared for stereotaxic injection using standard procedures approved by the Stanford University Administrative Panel on Laboratory Animal Care. Briefly, animals were anesthetized by intraperitoneal injection with a mixture of ketamine (60-80 mg/kg) and dexmedetomidine (0.6 mg/kg). A small craniotomy was performed over the desired viral injection site, and then a pulled glass pipette containing viral solution was lowered to the desired location. Stereotaxic injection coordinates were determined from bregma along the anterior-posterior (AP) and medial-lateral (ML) axes, and from the surface of the brain on the dorsal-ventral (DV) axis. Injection coordinates (in mm): motor cortex AP +0.2, ML +1.0, DV −0.8; OFC AP +2.6, ML +1.0, DV −1.8. For locomotor sensitization experiments, OFC

was injected bilaterally: AP +2.6, ML ±1.0, DV −1.8. Dorsal striatal coordinates were determined relative to bregma (in mm): AP +0.5, ML −2.0, DV −3.5. Viral solution (0.3-0.5 μL) was injected using a glass pipette connected to a Hamilton syringe (Hamilton Company 800 series, 5 μl capacity) and a microinjection pump (Harvard Apparatus) at a flow rate of 0.1 μL/min. To reduce backflow, the injection pipette was left in place for 5 minutes following infusion. The scalp was sutured using MICHEL staples (FST), Meloxicam (5 mg/kg) was injected subcutaneously to reduce pain following the surgery, and Antisedan (atipamezole) was injected (6 mg/kg) intraperitoneally to reverse the anesthesia effect of dexmedetomidine once the surgery was complete. Animals were monitored daily for abnormalities and received daily doses of Meloxicam (5 mg/kg SQ) for the 72 hours following surgical intervention. For RV experiments, animals received viral injections using parameters identical to those above. RV vectors were injected three weeks following Cre induction. Animals were allowed to recover for one week prior to sacrifice and tissue processing.

Cre Induction—Animals were timed to be 8-9 weeks old on the day of Cre induction. After recovering from AAV injection, animals were given four days of handling and injection habituation (0.1 ml saline) prior to induction of Cre recombination. On the following day, animals were given either a single dose of cocaine (30 mg/kg IP) or saline, paired with a dose of 4-hydroxytamoxifen (Sigma H6278, 50 mg/kg IP). 4-hydroxytamoxifen was first dissolved in 100% ethanol (20 mg/ml) at 37°C, then suspended in Chen oil (80% sunflower oil, 20% castor oil) by layering the ethanol solution on top of the Chen Oil in a 1.7 mL Eppendorf tube and evaporating the ethanol using a SpeedVac concentrator (ThermoFisher Scientific). The tube was then vortexed to distribute the 4-OHT evenly in the oil (final concentration 10 mg/ml, 5 ml/kg mouse). Following drug injection, animals were returned to their home cage. For chronic cocaine experiments, animals were induced in an identical fashion, but beginning three weeks prior to Cre induction, animals received 7 daily injections of either cocaine (15 mg/kg) or saline.

Implantation of Drug Cannulae—Following stereotaxic viral injection, holes were drilled in the skull (AP +0.6 mm, LM ±1.7 mm from bregma) for subsequent bilateral drug cannulae implantation. Small screws were bilaterally inserted partially into the skull (AP −4.0 mm, LM ± 1.0 mm) to improve subsequent cannula attachment. Cannulae (PlasticsOne, C235G-3.4/SPC 26 ga guide cannulae) were slowly inserted into the brain via stereotax arm, and then attached to the skull with C&B-Metabond dental cement (Parkell Inc.). After Metabond was dry to the touch, the guide cannula was further stabilized with the application of Geristore A+B dual cure resin ionomer (DenMat Holdings, Inc.). Once Geristore hardened, a dummy cannula (PlasticsOne C235DC/SPC DUMMY DBL.008”/.2MM) was inserted into the guide cannula to prevent contamination from entering the cranial cavity. An aluminum cap (PlasticsOne 303DC/1A DUST CAP 42476 ALUMINUM) was placed over the cannula to prevent the animal from potentially removing the dummy plug. Scalp skin was chemically sutured (3M Vetbond tissue adhesive) to encapsulate the base of the implant.

Tissue Processing and Imaging—At the end of the experimental time course, mice were heavily anesthetized with pentobarbital (50 mg/kg IP), followed by intracardial

perfusion with 4% paraformaldehyde (PFA) in phosphate buffer (0.1M, pH 7.4). PFA was allowed to circulate at a rate of ~5 ml/min for 3 minutes, followed by decapitation and brain isolation. Isolated brains were stored in PBS + 4% PFA overnight, then transferred to PBS + 0.02% sodium azide in preparation for tissue sectioning. Isolated brains were prepared with either a coronal or sagittal brain blocker and then fixed to a base plate. 50 μm sections (coronal or sagittal) were prepared with a vibratome (Leica VT1000S) and every third slice was directly mounted to a glass microscope slide. Other tissue groups were stored in PBS at 4°C for potential future use. Once dried, cover slips were applied to individual slides with mounting medium containing DAPI (ProLong Gold Antifade Mountant with DAPI, ThermoFisher Scientific) and allowed to cure in the dark for at least 48 hours. Whole slide images were then acquired at a resolution of 0.64 μm/pixel using an Olympus VS120 fluorescence slide scanner and manually analyzed via Olympus OlyVIA software available freely online. The investigator was blinded to experimental condition when technically feasible. Imaging parameters were identical across experimental condition. Confocal images were acquired using a Nikon Instruments A1 laser scanning confocal microscope and analyzed using FIJI image software (Schindelin et al., 2012).

By default, rabies tracing data were analyzed at 1:3 sampling density (1x 50 μm slice per 150 μm). If retrograde label was detected, but fewer than 10 neurons were found in any of the 11 major cortical divisions (Figure 2), a second group of tissue was mounted, imaged, and analyzed (2x 50μm slices per 150 μm), adding the third tissue group if necessary (all brain slices analyzed). Any individual cortical divisions that still had fewer than 10 retrogradely labeled neurons after complete tissue sampling were excluded from group statistical analysis. This step was particularly important to reduce the effects of small number variability on the proportions of active cells described in (Figures 3, 5, 7, and S3), increasing the precision of reported values for both cortical origin and Arc activation status. If more than 10,000 retrogradely labeled cortical neurons were detected when sampling at 1:3 density, tissue were analyzed at 1:9 density instead (1x 50 pμ slice per 450 μm). This reduces the precision of reported values for both cortical origin and Arc activation status, but is counterbalanced by the high total number of labeled input neurons. To avoid counting cortical neurons that were labeled nonspecifically, tissue along viral injection tracts and tissue that was visibly damaged was not analyzed. This yielded a slight undersampling of motor cortex inputs and an even smaller undersampling of somatosensory cortex inputs equally across all conditions.

Cortical area abbreviations consistent with Paxinos nomenclature: S1: primary somatosensory; S2: secondary somatosensory; M1: primary motor; M2: secondary motor; AI: agranular insular; GI/DI: granular/dysgranular insular; LO: lateral orbital; VO: ventral orbital; MO: medial orbital; PRl: prelimbic; Fra: frontal association; RSD: dysgranular retrosplenial; RSG: granular retrosplenial; Cg1: cingulate area 1; Cg2: cingulate area 2; V1: primary visual; V2: secondary visual; PtA: parietal association; Aud: auditory; PRh: perirhinal; Ent: entorhinal; Ect: ectorhinal; TeA: temporal association. *: layer/subregion undefined.

Cell Density Analysis—Density of Ai14-expressing neurons was assessed in FIJI software. Binary thresholding was applied to each slice to maximize contrast between

neuronal somata and neurite, and identical thresholding parameters were applied across experimental condition. The investigator was blinded to experimental condition for virtually all analyses. For striatal density analysis, 500 μm x 500 μm fields were extracted based on their relative laterality from midline. Dorsal striatum was segmented into thirds based on their maximum width along the medial-lateral axis to form medial (medial third), central (intermediate third), and lateral (lateral third) regions. Three fields were analyzed per striatal segment, with three slices analyzed per animal, across two animals. This yielded 18 segments per striatal region per condition. Depth calculations for cortical cell density were performed by extracting 50 μm columns perpendicular to the pial surface, starting at the pia and running to the terminus of cortical layer 6. Three columns were analyzed per slice per brain area, with three slices per animal and two animals per condition considered, yielding 18 cortical segments analyzed per condition per brain area. Intensity data were binned into 50 μm segments, then processed and graphed using OriginPro 2018 software (OriginLab Corporation). Signal to noise was calculated by measuring the integrated area under each curve and dividing cocaine signal by saline signal. Width of error bars and shaded contours represent ± 1 SEM.

Slice electrophysiology—21-28 days following stereotaxic injection of AAV, Arc-TRAP/Ai14 mice were anesthetized using isoflurane and sacrificed via decapitation. The brain was rapidly removed and placed into ice-cold high-sucrose cutting solution containing (in mM): 228 sucrose, 26 $NaHCO_3$, 11 glucose, 2.5 KCl, 1 NaH_2PO_4, 7 $MgSO_4$, and 0.5 $CaCl_2$. 250 μm sections of the injection sites (to verify injections) and the dorsal striatum were cut using a Leica vibratome in the sucrose cutting solution and were immediately transferred to an incubation chamber containing artificial cerebrospinal fluid (ACSF) consisting of (in mM): 119 NaCl, 26 NaHCO3, 11 dextrose, 2.5 KCl, 1 NaH_2PO_4, 1.3 $MgSO_4$, and 2.5 $CaCl_2$. The slices were allowed to recover at 32°C for 30 min before equilibrating at room temperature. To maintain optimal brain slice health during recordings, slices were placed in a recording chamber continuously perfused with heated ACSF (28-31°C) and gassed with 95% O_2 and 5% CO_2. Recordings were made using borosilicate glass pipettes (2.5-4.5 MΩ) filled with internal solution containing (in mM): 135 $CsMeSO_4$, 8 NaCl, 10 HEPES, 0.25 EGTA, 2 Mg_2ATP, 0.3 NaGTP, and 1 QX-314-Br (and 0.1 spermine for I/V measurements) (pH 7.3, 295 mOsm). For recordings measuring postsynaptic quantal amplitudes following evoked responses, $CaCl_2$ was removed from the ACSF and was replaced with an equal molarity of $SrCl_2$.

Data was collected using a Multiclamp 700B (Axon Instruments) and digitized using an ITC-18 (Instrutech Corp), filtered at 3 kHz and digitized at 10 kHz. Data was acquired and protocols were generated using Axograph-X software (Axograph). Optical stimulation (460 nm blue light) was delivered via the objective lens using a blue LED (Prizmatix). Electrical stimulation was generated using a Model 2100 Isolated Pulse Stimulator (A-M Systems) and delivered via a bipolar electrode (FHC) placed 200-500 μm from the patched cell. Dorsal striatal medium spiny neurons were identified visually using DIC imaging (Olympus BX51WI microscope). tdTomato positive and negative cells were identified visually using a 557 nm excitation/584 nm emission filter cube (Chroma).

For all electrophysiological data collection, patched cells were allowed to stabilize for at least 5 minutes prior to data collection. Cells that showed changes in series resistance of more than 20% during the course of recording were excluded from data analysis. In an effort to target recordings to MSNs, cells that demonstrated resting membrane potentials less hyperpolarized than −70 mV or had membrane resistances or input resistances larger than 300 MΩ were not used for data collection (<5% of cells). At least 30 trials/responses were averaged for each cell under each condition, and 5 seconds per evoked peak was allowed in between each trial. For paired-pulse ratio measurements, EPSCs were elicited with a 50 ms inter-peak interval. Paired-pulse ratio was calculated as the amplitude of the second peak / amplitude of the first peak. For AMPAR/NMDAR ratio measurements, EPSCs were evoked while holding medium spiny neurons at −70 mV (AMPAR) and then at +50 mV (NMDAR). The final ratio was calculated by taking the average maximum peak amplitude at −70 mV, and then dividing by the average response amplitude 40 ms after the +50 mV EPSC was evoked. Alternating sets of 30 trials at +50 mV and −70 mV were evoked in each cell. Series resistance stability was confirmed between each set of alternating trials of −70 mV or +50 mV. At least three consecutive sets of 30 trials were analyzed for each cell to ensure stable responses after switching between −70 mV and +50 mV voltage-clamp conditions. If the average amplitude of evoked responses shifted by more than 25% between similar trial sets, the cell was excluded from data analysis. Quantal amplitudes in the presence of strontium-containing ACSF were measured 30-200 ms following evoked stimulation.

Locomotor Sensitization—3-4 weeks after Cre induction, mice previously injected with AAV Cre-ON or Cre-OFF hM4Di were given IP injections of saline or cocaine (15 mg/kg) in their home cages 5 minutes prior to placement in open field locomotor chambers (Med Associates Inc.). Locomotor testing began once mice were placed into the chambers and lasted for 30 mins. Med Associates Activity Monitor software was used to track mouse movements based on infrared beam sensors in the chamber. Locomotor behavior data was validated both during collection and also following the test to ensure that all sensors, software, and system parts were functioning correctly. The total distance traveled during the 30 min test was used as a measure of locomotor behavior. Following the test, the mice were immediately returned to their home cages. This was repeated for a total of seven sessions with the following regimen: Day 1 saline only, Days 2-4 cocaine, Day 5 cocaine + CNO, Day 6 cocaine, Day 7 saline + CNO. Animals that showed a hypersensitization phenotype (cocaine day 2 > 200% cocaine day 1) were excluded from analysis to avoid motor ceiling effects. For systemic CNO experiments, 1 of 26 animals in the Cre-OFF condition were excluded from analysis under these criteria. For local CNO infusion experiments, 1 of 17 Cre-ON and 1 of 18 Cre-OFF animals were excluded under these criteria.

For IP CNO experiments, animals received a single IP injection (3 mg/kg) of CNO (Tocris Bioscience) on Days 5 and 7, 30 minutes prior to placement into the locomotor chambers. For experiments locally infusing CNO into the dorsal striatum, mice were restrained to remove the protective aluminum cap and dummy plug from the guide cannula. A bilateral injection cannula (PlasticsOne C235I/SPC INTERNAL DBL 38981 33GA, cut to protrude 1.5mm beyond guide cannula, reaching a depth of 3.5mm ventral to bregma) was then placed into the guide cannula. CNO (300 μM) was infused via microinfusion pump (Harvard

Apparatus, Inc.) and Hamilton syringes (Hamilton Company 800 series, 5 μl capacity) at a rate of 100 nl/min for 3 minutes. To prevent backflow, injection cannula were left for 1 minute subsequent to drug infusion, then removed. The dummy cannula and protective cap were then replaced, and the animal was returned to its home cage. As in systemic CNO experiments, mice received IP injections of saline or cocaine (15 mg/kg) 5 minutes prior to placement in locomotor assessment chambers, and were assessed using identical parameters.

For images of Cre-ON and Cre-OFF hM4Di injection sites, since experiments were performed in Arc-TRAP/Ai14 animals, red signal also arises from Arc-dependent tdTomato. Since viral-mediated fluorescence was generally much brighter than Arc-tdTomato, images were thresholded to maximally visualize viral injection site.

Capture of Locomotor Ensembles—To gain genetic access to neuronal populations activated by locomotion, mice were provided with wireless running wheels with magnetic movement sensors (Med Associates Inc.) in their home cages. Wheel and injection habituation started simultaneously, and mouse locomotor activity was monitored nightly using Med Associates software coupled to a wireless receiving hub. Animals were housed in a facility with a 12/12 hour light/dark cycle, with the dark cycle beginning at 7 pm and persisting until 7 am. Mice typically began running on the wheels within 30 minutes of dark cycle onset. Each animal was monitored until they reached a threshold of 200 meters run within the first 90 minutes of the dark cycle, or 500 meters total run over the course of the full dark cycle. Mice continued to receive daily injection habituation during this period. After four days of injection habituation AND reaching the designated locomotor threshold, mice were injected with 50 mg/kg IP 4-OHT 30-60 minutes prior to the onset of the dark cycle. Cohort-matched animals received 30 mg/kg IP cocaine and 50 mg/kg 4-OHT at the same time. Mice were allowed to locomote freely in their home cages overnight, and wheel running data were assessed the next day to verify that mice reached threshold wheel-based locomotor activity (200 meters during the first 90 minutes of the dark cycle), in addition to their basal locomotor activity (not measured). Running wheels were then removed from the cages and decontaminated. Mice that did not reach this locomotor threshold were excluded from further examination (1 of 6 mice for rabies tracing experiments and 1 of 10 mice for electrophysiology experiments).

QUANTIFICATION AND STATISTICAL ANALYSIS

Standard statistical software packages in Microsoft Excel, OriginPro, and GraphPad Prism were utilized for analysis. Unless specified otherwise, all data are shown as mean ± 1 SEM. Numerical results of statistical tests, including Student’s t-test, one-way ANOVA, two-way ANOVA, and chi-squared tests, are reported in the figure legends, with significance markers in figures, and adjusted for multiple comparisons when appropriate. Multiple comparison adjustments included Bonferroni correction (t-test) and Dunnett’s, Tukey’s, and Sidak’s post-hoc tests (one-way and two-way ANOVA).

DATA AND CODE AVAILABILITY

Source data for all rabies tracing experiments are available in Supplemental Excel File 1. Other datasets supporting the current study have not been deposited in a public repository

due to file size and proprietary file format restrictions, but are available from the corresponding author on request.

Supplementary Material

Refer to Web version on PubMed Central for supplementary material.

ACKNOWLEDGEMENTS

We thank Casey Guenthner for providing animals and initial feedback on using the TRAP system and the Stanford Gene Vector and Virus Core for consultation and production of viruses. This work was supported by grants from the Stanford University Wu Tsai Neurosciences Institute and NIH grants P50 DA042012, F32 DA038913, K999 DA041445, T32 NS007280-29, and T32 NS007280-30.

REFERENCES

Albisetti GW, Ghanem A, Foster E, Conzelmann KK, Zeilhofer HU, and Wildner H (2017). Identification of two classes of somatosensory neurons that display resistance to retrograde infection by rabies virus. J. Neurosci 37, 10358–10371. [PubMed: 28951448]

Allen WE, DeNardo LA, Chen MZ, Liu CD, Loh KM, Fenno LE, Ramakrishnan C, Deisseroth K, and Luo L (2017). Thirst-associated preoptic neurons encode an aversive motivational drive. Science 357, 1149–1155. [PubMed: 28912243]

Beier KT, Kim CK, Hoerbelt P, Hung LW, Heifets BD, DeLoach KE, Mosca TJ, Neuner S, Deisseroth K, Luo L, and Malenka RC (2017). Rabies screen reveals GPe control of cocaine-triggered plasticity. Nature 549, 345–350. [PubMed: 28902833]

Beier KT, Steinberg EE, DeLoach KE, Xie S, Miyamichi K, Schwarz L, Gao XJ, Kremer EJ, Malenka RC, and Luo L (2015). Circuit architecture of VTA dopamine neurons revealed by systematic input-output mapping. Cell 162, 622–634. [PubMed: 26232228]

Bramham CR, Alme MN, Bittins M, Kuipers SD, Nair RR, Pai B, Panja D, Schubert M, Soule J, Tiron A, and Wibrand K (2010). The Arc of synaptic memory. Exp. Brain. Res 200, 125–140. [PubMed: 19690847]

Caprioli D, Venniro M, Zhang M, Bossert JM, Warren BL, Hope BT, and Shaham Y (2017). Role of dorsomedial striatum neuronal ensembles in incubation of methamphetamine craving after voluntary abstinence. J. Neurosci 37, 1014–1027. [PubMed: 28123032]

Choi JH, Sim SE, Kim JI, Choi DI, Oh J, Ye S, Lee J, Kim T, Ko HG, Lim CS, and Kaang BK (2018). Interregional synaptic maps among engram cells underlie memory formation. Science 360, 430–435. [PubMed: 29700265]

Cruz FC, Javier Rubio F, and Hope BT (2015). Using c-fos to study neuronal ensembles in corticostriatal circuitry of addiction. Brain Res. 1628, 157–173. [PubMed: 25446457]

Cruz FC, Koya E, Guez-Barber DH, Bossert JM, Lupica CR, Shaham Y, and Hope BT (2013). New technologies for examining the role of neuronal ensembles in drug addiction and fear. Nat. Rev. Neurosci 14, 743–754. [PubMed: 24088811]

DeNardo LA, Liu CD, Allen WE, Adams EL, Friedmann D, Fu L, Guenthner CJ, Tessier-Lavigne M, and Luo L (2019). Temporal evolution of cortical ensembles promoting remote memory retrieval. Nat. Neurosci 22, 460–469. [PubMed: 30692687]

Girasole AE, Lum MY, Nathaniel D, Bair-Marshall CJ, Guenthner CJ, Luo L, Kreitzer AC, and Nelson AB (2018). A subpopulation of striatal neurons mediates levodopa-induced dyskinesia. Neuron 97, 787–795. [PubMed: 29398356]

Gomez JL, Bonaventura J, Lesniak W, Mathews WB, Sysa-Shah P, Rodriguez LA, Ellis RJ, Richie CT, Harvey BK, Dannals RF, et al. (2017). Chemogenetics revealed: DREADD occupancy and activation via converted clozapine. Science 357, 503–507. [PubMed: 28774929]

Guenthner CJ, Miyamichi K, Yang HH, Heller HC, and Luo L (2013). Permanent genetic access to transiently active neurons via TRAP: targeted recombination in active populations. Neuron 78, 773–784. [PubMed: 23764283]

Josselyn SA, and Frankland PW (2018). Memory allocation: mechanisms and function. Annu. Rev. Neurosci 41, 389–413. [PubMed: 29709212]

Koya E, Cruz FC, Ator R, Golden SA, Hoffman AF, Lupica CR, and Hope BT (2012). Silent synapses in selectively activated nucleus accumbens neurons following cocaine sensitization. Nat. Neurosci 15, 1556–1562. [PubMed: 23023294]

Koya E, Golden SA, Harvey BK, Guez-Barber DH, Berkow A, Simmons DE, Bossert JM, Nair SG, Uejima JL, Marin MT, et al. (2009). Targeted disruption of cocaine-activated nucleus accumbens neurons prevents context-specific sensitization. Nat. Neurosci 12, 1069–1073. [PubMed: 19620976]

Krashes MJ, Koda S, Ye C, Rogan SC, Adams AC, Cusher DS, Maratos-Flier E, Roth BL, and Lowell BB (2011). Rapid, reversible activation of AgRP neurons drives feeding behavior in mice. J. Clin. Invest 121, 1424–1428. [PubMed: 21364278]

Li X, Rubio FJ, Zeric T, Bossert JM, Kambhampati S, Cates HM, Kennedy PJ, Liu QR, Cimbro R, Hope BT, et al. (2015). Incubation of methamphetamine craving is associated with selective increases in expression of Bdnf and Trkb, glutamate receptors, and epigenetic enzymes in cue-activated Fos-expressing dorsal striatal neurons. J. Neurosci 35, 8232–8244. [PubMed: 26019338]

Luo L, Callaway EM, and Svoboda K (2008). Genetic dissection of neural circuits. Neuron 57, 634–660. [PubMed: 18341986]

Luo L, Callaway EM, and Svoboda K (2018). Genetic dissection of neural circuits: a decade of progress. Neuron 98, 256–281. [PubMed: 29673479]

Madisen L, Zwingman TA, Sunkin SM, Oh SW, Zariwala HA, Gu H, Ng LL, Palmiter RD, Hawrylycz MJ, Jones AR, et al. (2010). A robust and high-throughput Cre reporting and characterization system for the whole mouse brain. Nat. Neurosci 13, 133–140. [PubMed: 20023653]

Miyamichi K, Shlomai-Fuchs Y, Shu M, Weissbourd BC, Luo L, and Mizrahi A (2013). Dissecting local circuits: parvalbumin interneurons underlie broad feedback control of olfactory bulb output. Neuron 80, 1232–1245. [PubMed: 24239125]

Oliet SH, Malenka RC, and Nicoll RA (1996). Bidirectional control of quantal size by synaptic activity in the hippocampus. Science 271, 1294–1297. [PubMed: 8638114]

Pierce RC, Reeder DC, Hicks J, Morgan ZR, and Kalivas PW (1998). Ibotenic acid lesions of the dorsal prefrontal cortex disrupt the expression of behavioral sensitization to cocaine. Neuroscience 82, 1103–1114. [PubMed: 9466434]

Ramirez S, Liu X, Lin PA, Suh J, Pignatelli M, Redondo RL, Ryan TJ, and Tonegawa S (2013). Creating a false memory in the hippocampus. Science 341, 387–391. [PubMed: 23888038]

Robinson TE, and Berridge KC (2003). Addiction. Annu. Rev. Psychol 54, 25–53. [PubMed: 12185211]

Rubio FJ, Liu QR, Li X, Cruz FC, Leao RM, Warren BL, Kambhampati S, Babin KR, McPherson KB, Cimbro R, et al. (2015). Context-induced reinstatement of methamphetamine seeking is associated with unique molecular alterations in Fos-expressing dorsolateral striatum neurons. J. Neurosci 35, 5625–5639. [PubMed: 25855177]

Ryan TJ, Roy DS, Pignatelli M, Arons A, and Tonegawa S (2015). Engram cells retain memory under retrograde amnesia. Science 348, 1007–1013. [PubMed: 26023136]

Saunders A, Johnson CA, and Sabatini BL (2012). Novel recombinant adeno-associated viruses for Cre activated and inactivated transgene expression in neurons. Front. Neural Circuits 6, 47. [PubMed: 22866029]

Schindelin J, Arganda-Carreras I, Frise E, Kaynig V, Longair M, Pietzsch T, Preibisch S, Rueden C, Saalfeld S, Schmid B, et al. (2012). Fiji: an open-source platform for biological-image analysis. Nat. Methods 9, 676–682. [PubMed: 22743772]

Schoenbaum G, Saddoris MP, Ramus SJ, Shaham Y, and Setlow B (2004). Cocaine-experienced rats exhibit learning deficits in a task sensitive to orbitofrontal cortex lesions. Eur. J. Neurosci 19, 1997–2002. [PubMed: 15078575]

Steketee JD (2005). Cortical mechanisms of cocaine sensitization. Crit. Rev. Neurobiol 17, 69–86. [PubMed: 16808728]

Tonegawa S, Morrissey MD, and Kitamura T (2018). The role of engram cells in the systems consolidation of memory. Nat. Rev. Neurosci 19, 485–498. [PubMed: 29970909]

Valjent E, Bertran-Gonzalez J, Aubier B, Greengard P, Herve D, and Girault JA (2010). Mechanisms of locomotor sensitization to drugs of abuse in a two-injection protocol. Neuropsychopharmacol. 35, 401–415.

Vanderschuren LJ, and Kalivas PW (2000). Alterations in dopaminergic and glutamatergic transmission in the induction and expression of behavioral sensitization: a critical review of preclinical studies. Psychopharmacology (Berl.) 151, 99–120. [PubMed: 10972458]

Vezina P (2007). Sensitization, drug addiction and psychopathology in animals and humans. Prog. Neuropsychopharmacol. Biol. Psychiatry 31, 1553–1555. [PubMed: 17900776]

Wall NR, De La Parra M, Callaway EM, and Kreitzer AC (2013). Differential innervation of direct- and indirect-pathway striatal projection neurons. Neuron 79, 347–360. [PubMed: 23810541]

Wall NR, Wickersham IR, Cetin A, De La Parra M, and Callaway EM (2010). Monosynaptic circuit tracing in vivo through Cre-dependent targeting and complementation of modified rabies virus. Proc. Natl. Acad. Sci. USA 107, 21848–21853. [PubMed: 21115815]

Whitaker LR, Carneiro de Oliveira PE, McPherson KB, Fallon RV, Planeta CS, Bonci A, and Hope BT (2016). Associative learning drives the formation of silent synapses in neuronal ensembles of the nucleus accumbens. Biol. Psychiatry 80, 246–256. [PubMed: 26386479]

Whitaker LR, and Hope BT (2018). Chasing the addicted engram: identifying functional alterations in Fos-expressing neuronal ensembles that mediate drug-related learned behavior. Learn. Mem 25, 455–460. [PubMed: 30115767]

Wickersham IR, Finke S, Conzelmann KK, and Callaway EM (2007). Retrograde neuronal tracing with a deletion-mutant rabies virus. Nat. Methods 4, 47–49. [PubMed: 17179932]

Winstanley CA, Green TA, Theobald DE, Renthal W, LaPlant Q, DiLeone RJ, Chakravarty S, and Nestler EJ (2009). DeltaFosB induction in orbitofrontal cortex potentiates locomotor sensitization despite attenuating the cognitive dysfunction caused by cocaine. Pharmacol. Biochem. Behav 93, 278–284. [PubMed: 19135469]

Wolf ME (1998). The role of excitatory amino acids in behavioral sensitization to psychomotor stimulants. Prog. Neurobiol 54, 679–720. [PubMed: 9560846]

Wolf ME, and Ferrario CR (2010). AMPA receptor plasticity in the nucleus accumbens after repeated exposure to cocaine. Neurosci. Biobehav. Rev 35, 185–211. [PubMed: 20109488]

Ye L, Allen WE, Thompson KR, Tian Q, Hsueh B, Ramakrishnan C, Wang AC, Jennings JH, Adhikari A, Halpern CH, et al. (2016). Wiring and molecular features of prefrontal ensembles representing distinct experiences. Cell 165, 1776–1788. [PubMed: 27238022]

Zhang Z, Ferretti V, Guntan I, Moro A, Steinberg EA, Ye Z, Zecharia AY, Yu X, Vyssotski AL, Brickley SG, et al. (2015). Neuronal ensembles sufficient for recovery sleep and the sedative actions of alpha2 adrenergic agonists. Nat. Neurosci 18, 553–561. [PubMed: 25706476]

Ziminski JJ, Hessler S, Margetts-Smith G, Sieburg MC, Crombag HS, and Koya E (2017). Changes in appetitive associative strength modulates nucleus accumbens, but not orbitofrontal cortex neuronal ensemble excitability. J. Neurosci 37, 3160–3170. [PubMed: 28213443]

Zucker RS, and Regehr WG (2002). Short-term synaptic plasticity. Annu. Rev. Physiol 64, 355–405. [PubMed: 11826273]

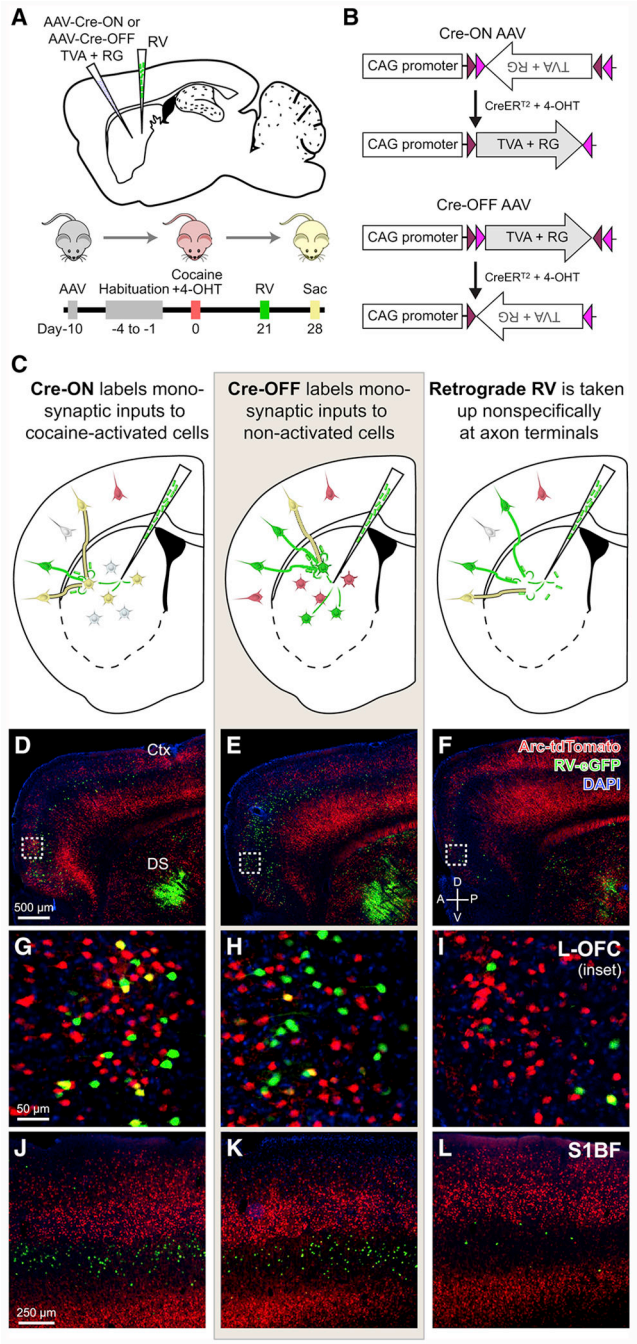

Figure 1. Cre-ON and Cre-OFF Vectors Enable Targeting of Complementary Striatal Populations for Monosynaptic Rabies Virus Tracing.

(A) Complementary targeting strategy for labeling monosynaptic inputs to cocaine-activated (Cre-ON) or non-activated (Cre-OFF) DS neurons.

(B) Cre-ON and Cre-OFF expression systems for selective expression of TVA and RG.

(C) Labeling of monosynaptic inputs to either cocaine-activated (Cre-ON, left) neurons or non-activated (Cre-OFF, middle) neurons. Corticostriatal projection patterns are also assessed using RV as a traditional retrograde tracer ([RG]RV-ΔG-eGFP) that is taken up nonselectively at axon terminals in the DS (right).

(D-F) Fluorescence images of Arc-dependent tdTomato expression (red), RV-infected neurons (green), and DAPI (blue) in cocaine-exposed animals previously injected with either Cre-ON (D) or Cre-OFF (E) AAVs followed by monosynaptic RV, or with no AAVs and retrograde RV alone(F). Scale bar applies to (D-F).

(G-I) Insets of hatched squares in (D-F). Monosynaptic inputs to cocaine-activated DS neurons are labeled green, while all cocaine-activated neurons are labeled red. Coincident label (yellow) indicates cocaine-activated cortical neurons that form direct connections to the targeted DS neuronal population. Scale bar applies to (G-I).

(J-L) Retrograde label in mouse barrel cortex for Cre-ON (J), Cre-OFF (K), and retrograde RV(L) conditions. Scale bar applies to (J-L).

See also Figures S1 and S2.

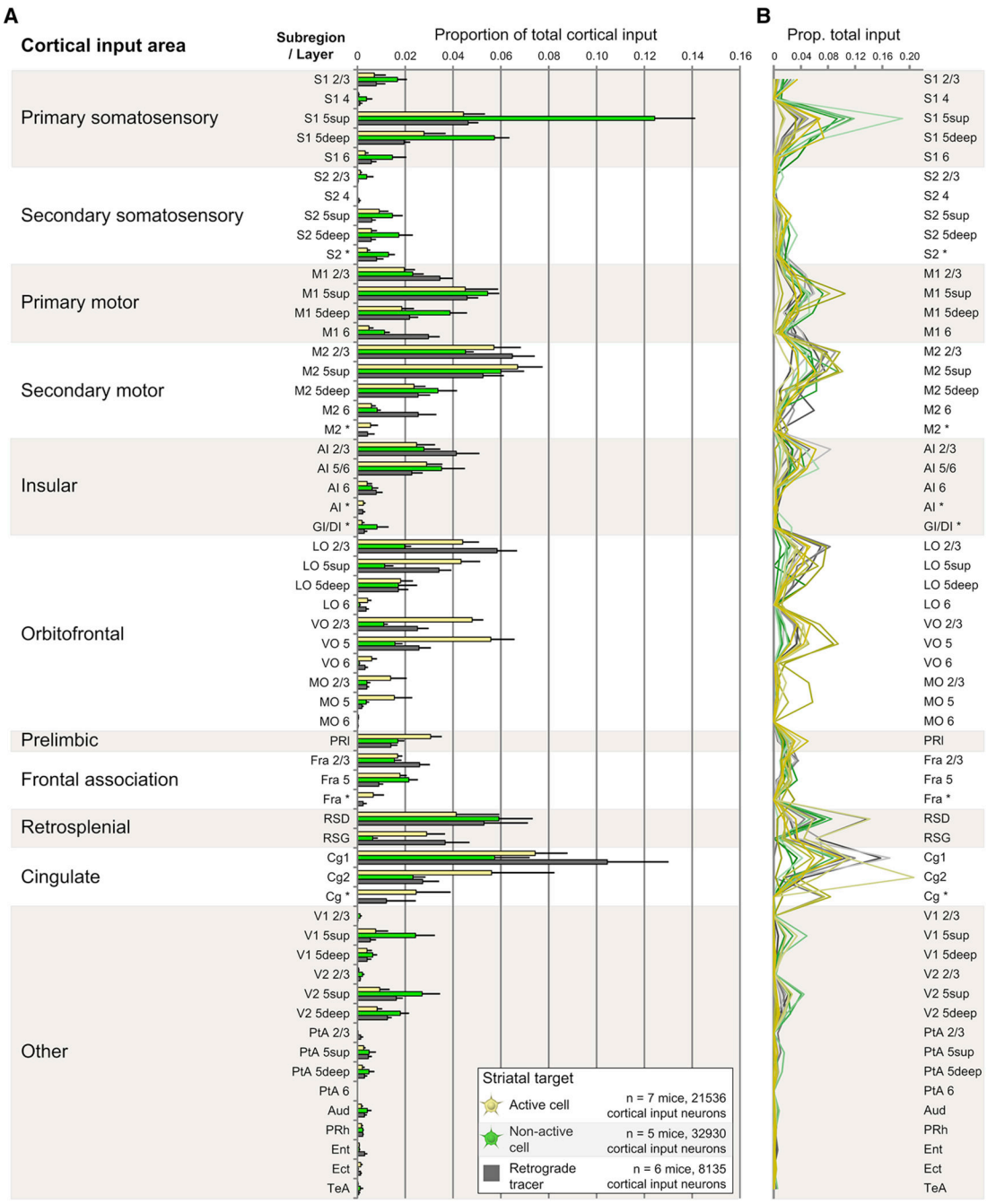

Figure 2. Cocaine-activated and Non-activated Striatal Neurons Receive Monosynaptic Inputs from Similar Sets of Cortical Input Areas.

(A) Origins of ALL cortical projections to cocaine-activated DS neurons (yellow), non-activated cells (green), or to DS nonspecifically (gray). Data are shown as mean ± 1 SEM. Significant interaction effect $F(114, 870)=2.836$, $p < 0.001$. Cre-ON different from Cre-OFF AND Retrograde RV in the following regions (p values multiplicity-adjusted via Dunnett's test): VO 2/3 (ON vs. OFF $p < 0.001$, ON vs. Retrograde $p=0.02$), VO 5 (ON vs. OFF $p < 0.001$, ON vs. Retrograde $p=0.001$), and Cg2 (ON vs. OFF $p < 0.001$, ON vs. Retrograde $p=0.002$). Cortical nomenclature consistent with Paxinos atlas (see STAR*Methods).

(B) As in (A), except rather than displaying population averages, each individual mouse is represented by a colored line.
See also Supplemental Excel File 1.

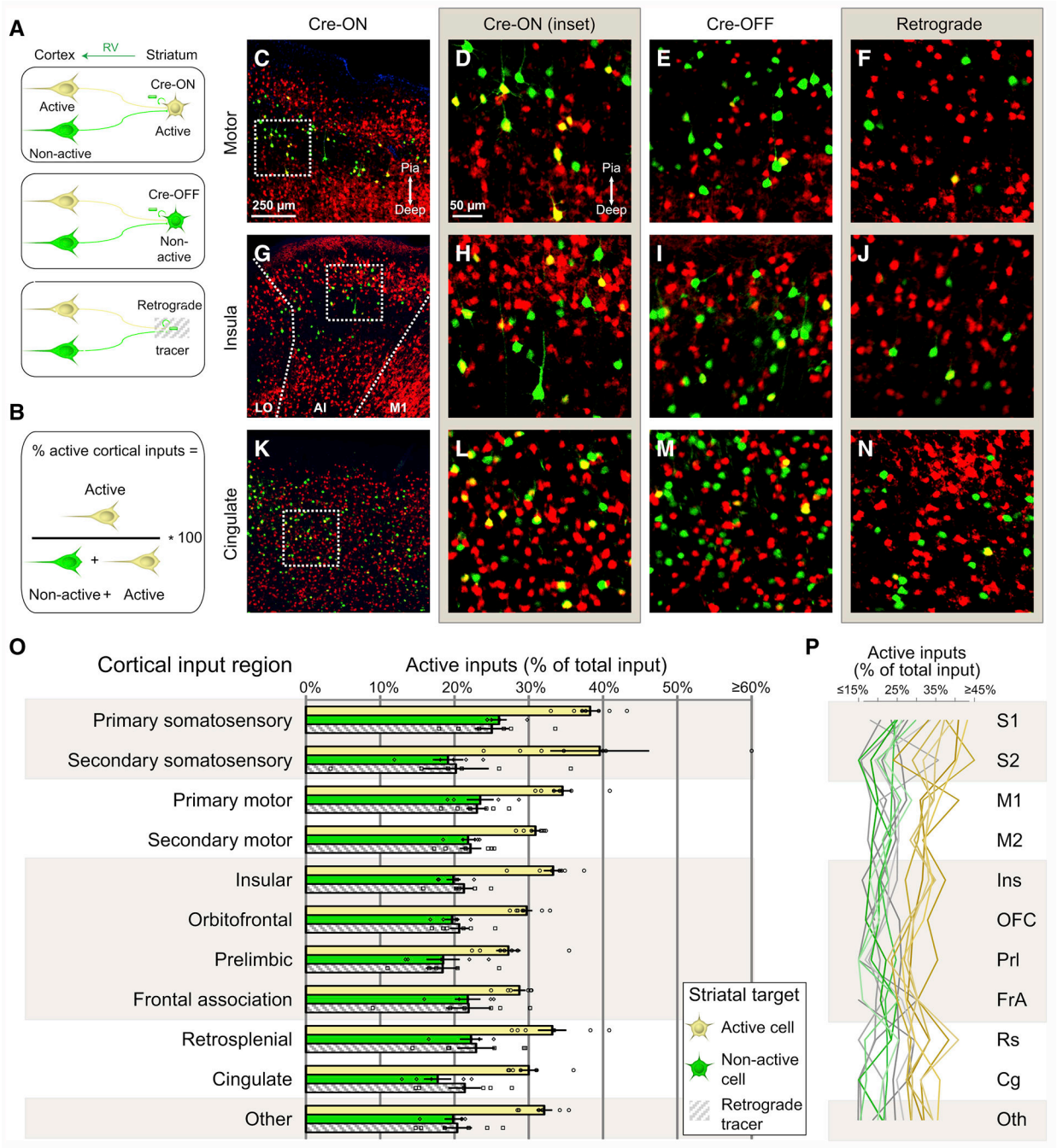

Figure 3. Cocaine-Activated Striatal Neurons Receive Preferential Input from Broadly Distributed Populations of Co-activated Cortical Neurons

(A) Schematic diagram applicable to the remainder of the figure. Cocaine activated and non-activated neurons are labeled yellow and green, respectively.

(B) Formula used in (O-P) to determine the proportion of active inputs originating from different cortical regions. Proportions were determined by dividing the number of cocaine-activated, rabies-labeled inputs by the total number of rabies-labeled neurons.

(C) Fluorescence image of motor cortex in a Cre-ON animal. Scale bar applies to (C, G, K). Images in (C-N) are oriented such that more superficial cortex is up and deeper cortex is down.

(D) High magnification inset of hatched box in (C), showing individual cortical input neurons either cocaine-activated (yellow) or non-activated (green). Scale bar applies to (D-F, H-J, and L-N).

(E-F) High magnification view of motor cortex in Cre-OFF and Retrograde conditions, respectively.

(G-J) As in (C-F), except for anterior insular cortex.

(K-N) As in (C-F), except for cingulate cortex.

(O) Proportion of activated cortical input neurons to targeted DS neurons that are activated or not activated by cocaine, or to dorsal striatum nonspecifically. Each individual data point represents the proportion of active inputs for a single animal. Bars indicate mean ± 1 SEM. Treatment groups significantly different via two-way ANOVA, $F(2,164)=102.5$, $p<0.001$. Cre-ON significantly different from Cre-OFF ($p<0.001$), Cre-ON significantly different from Retrograde ($p<0.001$), Cre-OFF vs. Retrograde n.s. ($p=0.78$) via Tukey's multiple comparisons test. For Cre-ON vs. Cre-OFF and Cre-ON vs. Retrograde, each individual cortical region except frontal association significantly different, multiplicity corrected $p<0.05$. Correction takes into account the partial use of Cre-ON data in Figure 7.

(P) As in (O), but with all applicable data points for an individual animal charted as a single line.

See also Figure S3.

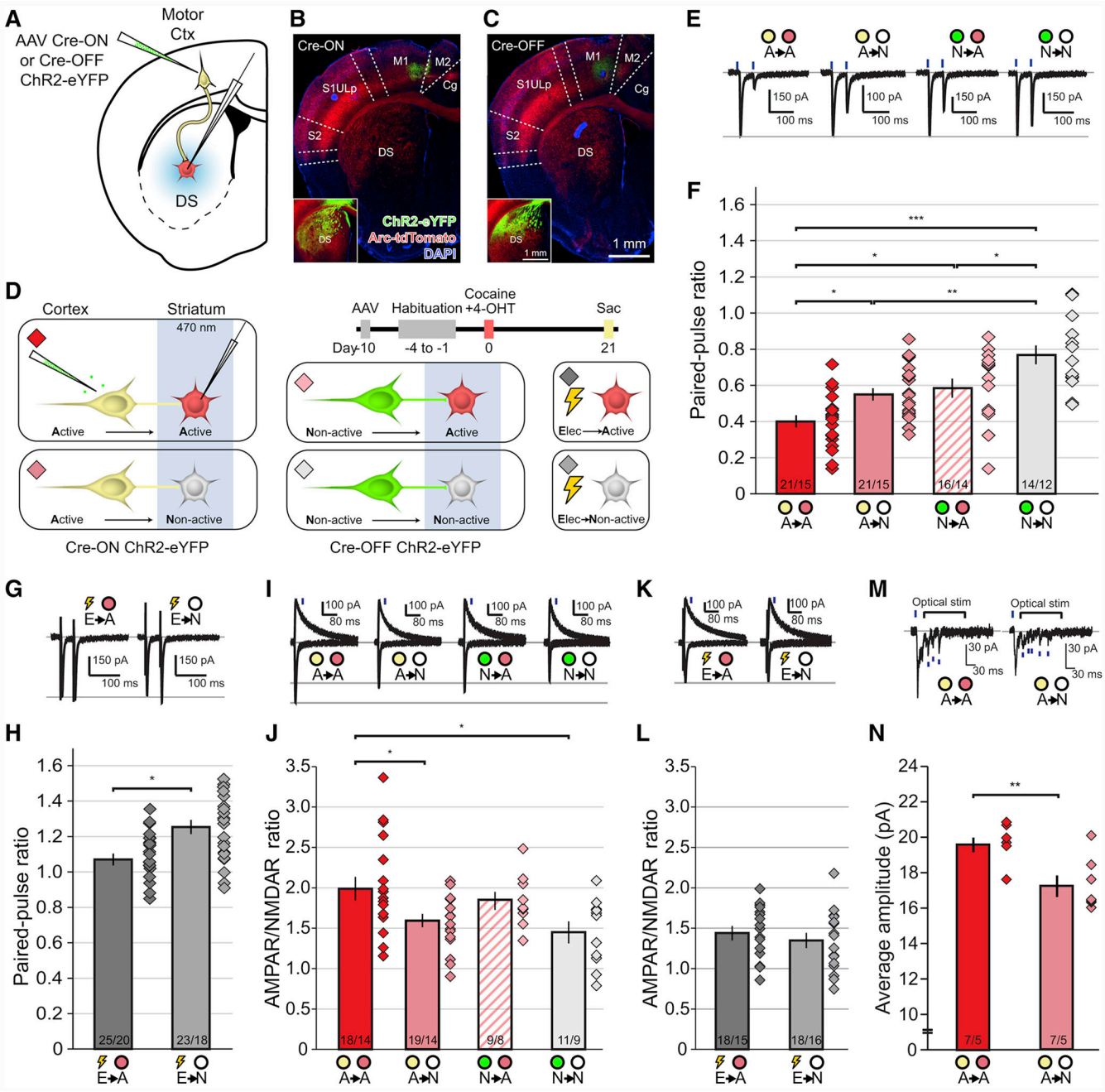

Figure 4. Enhanced Synaptic Strength Between Cocaine-activated Corticostriatal Neurons and Co-activated Striatal Cells

(A) Complementary targeting strategy for optogenetic stimulation of axon terminals and electrophysiological recording from downstream DS neurons.

(B) Injection site of AAV Cre-ON ChR2-eYFP into motor cortex, with high-exposure inset showing fibers in DS.

(C) As in B, but for Cre-OFF ChR2. Scale bars apply to (B-C).

(D) Timeline and targeting strategy for stimulating axon terminals arising from either cocaine-activated (Cre-ON ChR2, yellow) or non-activated (Cre-OFF ChR2, green) motor

corticostriatal neurons while recording from either cocaine-activated (red) or non-activated (gray) DS neurons. Nonspecific electrical stimulation was also performed while recording from cocaine-activated or non-activated DS neurons. Diamonds indicate recording conditions, matched to all subsequent panels.

(E) Representative EPSCs in response to paired-pulse optogenetic activation of corticostriatal axons while recording from either cocaine-activated or non-activated DS neurons.

(F) Paired-pulse ratios for all active and non-active synapse conditions. Diamonds illustrate ratio for individual cells. (Means significantly different via one-way ANOVA $F(3,68)=12.49$; A→A vs A→N, A→A vs N→A, N→A vs N→N: $p<0.05$; A→N vs N→N: $p<0.01$; A→A vs N→N $p<0.001$, Tukey's post-hoc test).

(G) Representative EPSCs in response to paired-pulse electrical stimulation. (E→A vs E→N: $t(46)=2.63$, $p<0.05$, two-tailed t-test).

(H) Electrically evoked paired-pulse ratios for all active and non-active synapse conditions.

(I) Representative EPSCs at −70 mV and +50 mV generated by optogenetic stimulation of corticostriatal axons. Blue lines indicate time at which measurements were made for NMDAR EPSCs.

(J) AMPAR/NMDAR ratios for all recording conditions. (Means different via one-way ANOVA, $F(3, 53) = 3.24$; A→A vs A→N, A→A vs N→N $p<0.05$, Dunnett's post-hoc test).

(K) Representative EPSCs at −70 mV and +50 mV generated by local electrical stimulation.

(L) AMPAR/NMDAR ratios for all electrical recording conditions. (E→A vs E→N: $t(34)=0.9720$, $p=0.34$).

(M) Representative traces of Sr^{2+}-mediated asynchronous miniature EPSCs (blue lines) when optogenetically stimulating cocaine-activated motor corticostriatal neurons while recording from either cocaine-activated or non-activated DS neurons.

(N) Amplitude of miniature EPSCs for all recording conditions. (A→A vs A→N: $t(12)=3.424$, $p=0.005$).

* $p<0.05$, ** $p<0.01$, *** $p<0.001$; n/m values at bottom of bars in (F, H, J, L, N) indicate neurons/animals. Bars indicate mean ± 1 SEM.

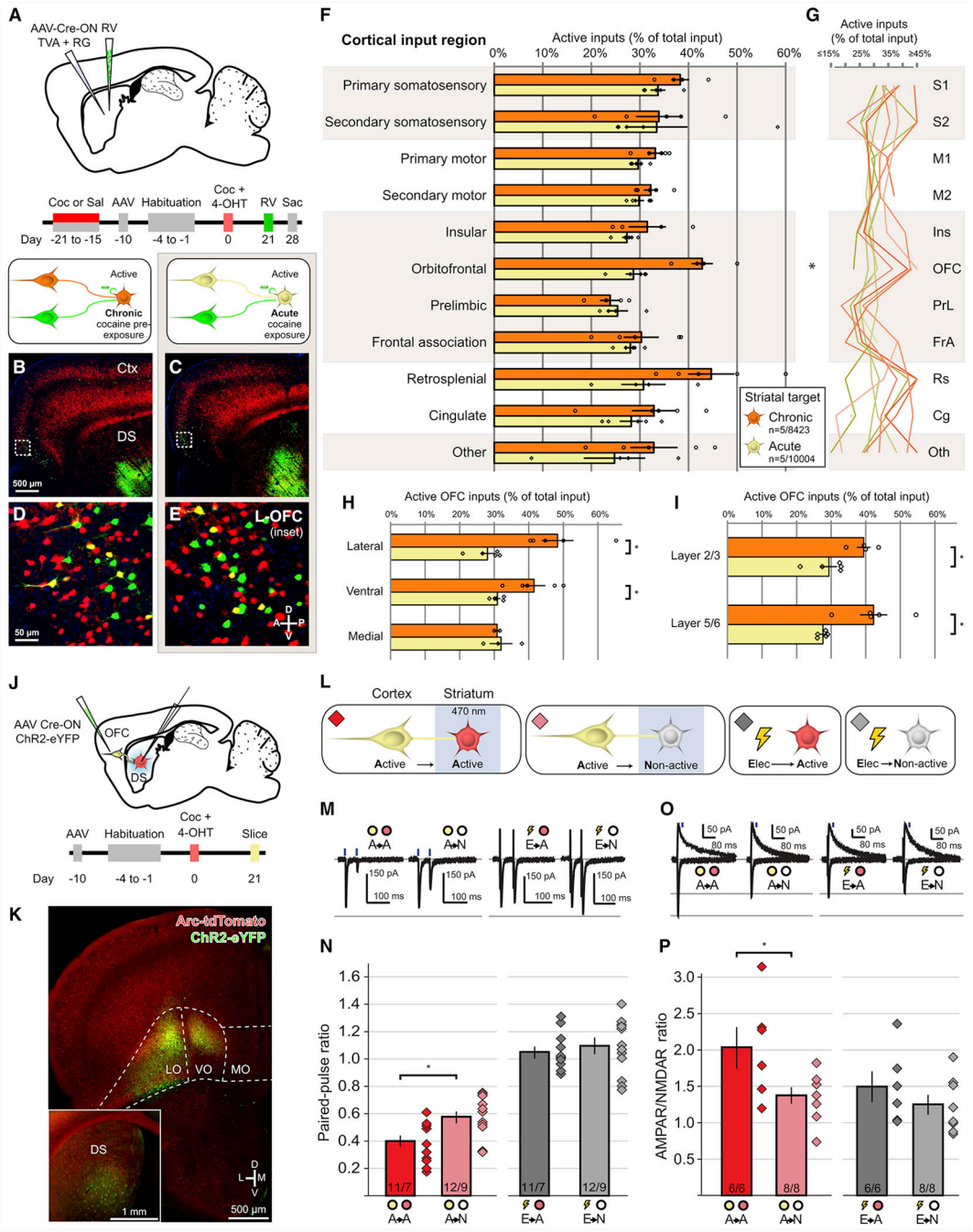

Figure 5. Chronic Cocaine Enhances the Connectivity Between Cocaine-activated OFC Neurons and Cocaine-activated Striatal Neurons

(A) Strategy and timeline for assessing monosynaptic connectivity to cocaine-activated DS neurons in animals previously exposed to 1 week of cocaine or saline beginning 3 weeks prior to acute cocaine challenge.

(B-C) Arc-dependent tdTomato expression (red) and RV-labeled neurons (green) in mice exposed to chronic cocaine (B) or to acute cocaine (C). Scale bar applies to (B-C).

(D-E) Inset of hatched squares in (B-C), depicting monosynaptic cortical inputs arising from OFC. Scale bar applies to (D-E).

(F) Proportion of monosynaptic inputs onto cocaine-activated DS neurons arising from cocaine-activated corticostriatal neurons in response to acute cocaine treatment in animals that had previously been administered cocaine (chronic, n=5 animals, 8423 neurons) or saline (acute, n=5 animals, 10004 neurons). All bars in this figure indicate mean ± 1 SEM. Treatment groups significantly different via two-way ANOVA, Chronic vs. Acute: $F(1,83) = 13.38$, $p<0.001$. OFC means significantly different (multiplicity-adjusted $p=0.03$ using Sidak's method).

(G) Individual animal data displayed in (F), where each animal is a separate line.

(H) Chronic cocaine pre-exposure enhances connectivity of cocaine-activated neurons in lateral and ventral OFC (Lateral: $t(8)=4.086$, $p=0.01$, Ventral: $t(8)=3.203$, $p=0.02$ adjusted using Sidak's method).

(I) Chronic cocaine pre-exposure enhances connectivity of cocaine-activated OFC neurons across cortical layers (OFC Layer 2/3: $t(7)=3.232$, $p=0.01$; OFC Layer 5/6: $t(8)=3.716$, $p=0.01$ adjusted using Sidak's method).

(J) Strategy and timeline for assessing synaptic connectivity arising from cocaine-activated OFC neurons to complementary populations of DS neurons.

(K) Injection site of Cre-ON ChR2 into OFC, with high-exposure inset showing fibers in DS.

(L) Strategy for recording responses between cocaine-activated OFC corticostriatal neurons (yellow) and either cocaine-activated (red) or non-activated (gray) DS neurons, as well as synaptic responses to electrical stimulation.

(M) Representative EPSCs in response to paired-pulse optogenetic or electrical activation of corticostriatal axons while recording from either cocaine-activated or non-activated DS neurons.

(N) Paired-pulse ratios for all recording conditions (A→A vs A→N: $t(21)=2.80$, $p=0.01$; E→A vs E→N: $t(21)=0.66$, $p=0.52$).

(O) Representative EPSCs at −70 mV and +50 mV generated by optogenetic or electrical stimulation of corticostriatal axons.

(P) AMPAR/NMDAR ratios for all recording conditions (A→A vs A→N: $t(12)=2.35$, $p=0.04$; E→A vs E→N: $t(12)=1.05$, $p=0.32$).

* $p<0.05$, ** $p<0.01$; n/m values at bottom of bars in (N, P) indicate neurons/animals. See also Figure S4.

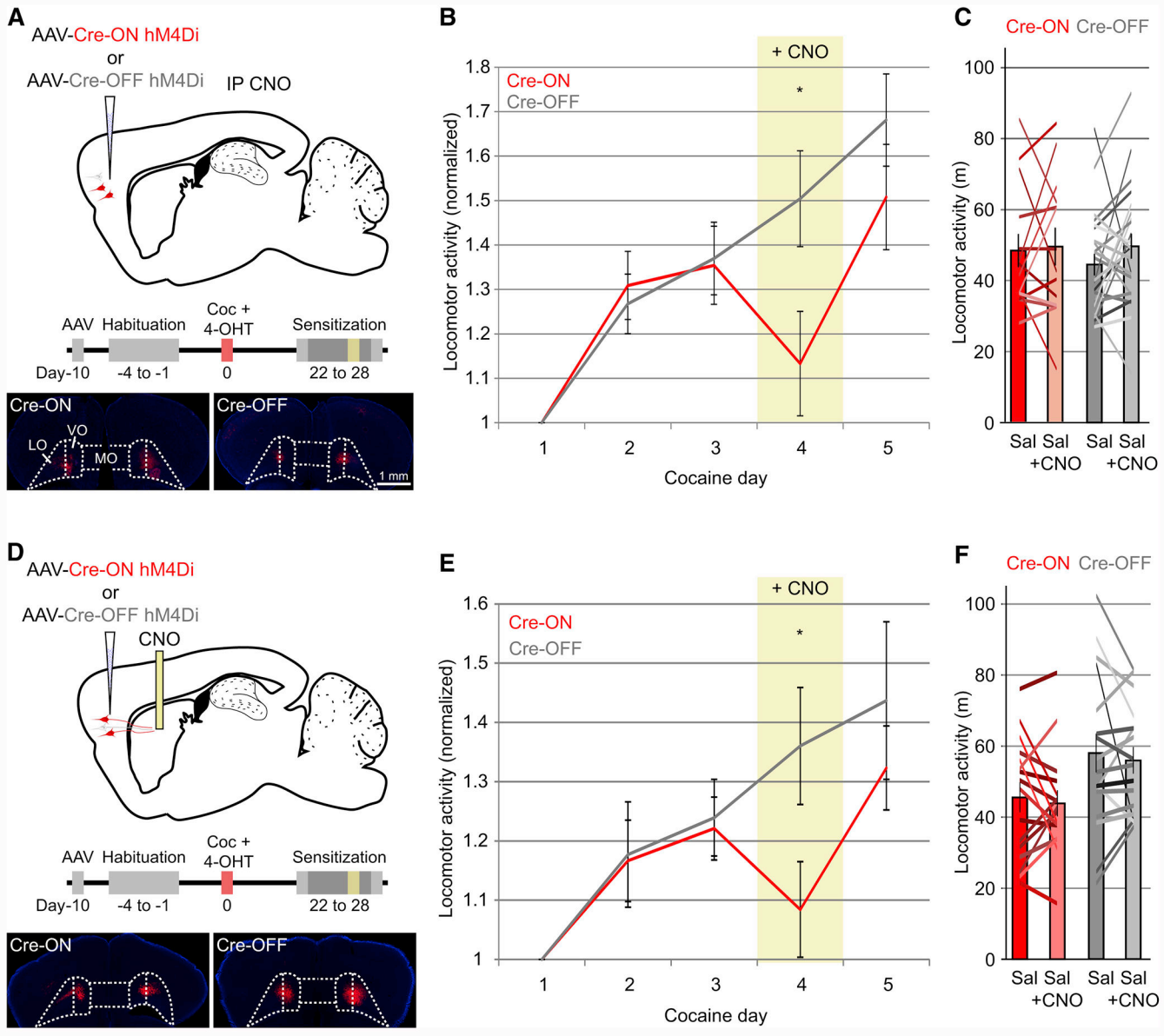

Figure 6. Chemogenetic Inhibition of Cocaine-activated Corticostriatal Neurons or Axons in DS Inhibits Locomotor Sensitization

(A) Complementary targeting strategy to chemogenetically inhibit either cocaine-activated (Cre-ON-hM4Di, n=15, red) or non-activated OFC neurons (Cre-OFF-hM4Di, n=25, gray). Bilateral injection sites for Cre-ON and Cre-OFF hM4Di-mCherry are displayed. Scale bars apply to (A,D).

(B) CNO blunts locomotor sensitization in mice injected with Cre-ON hM4Di (red, cocaine day 4, indicated by yellow column), whereas sensitization proceeds normally in animals injected with Cre-OFF hM4Di. Locomotor activity is normalized to the first cocaine day of sensitization (Cre-ON vs. Cre-OFF Day 4: $t(38)=2.23$, $p=0.03$). Error bars indicate ± 1 SEM, and apply to (B,E).

(C) CNO alone does not decrease basal locomotor activity in either group (Cre-ON: paired two-tailed $t(13)=0.23$, $p=0.81$; Cre-OFF: $t(22)=1.41$, $p=0.17$). Columns indicate population

mean, with error bar ± 1 SEM, and apply to (C,F). Colored lines indicate individual animal locomotion.

(D) Complementary targeting strategy to chemogenetically inhibit either cocaine-activated (Cre-ON-hM4Di, n=16, red) or non-activated (Cre-OFF-hM4Di, n=17, gray) OFC axons in DS.

(E) Local CNO infusion into the DS blunts locomotor sensitization when inhibiting axons arising from cocaine-activated OFC neurons (red, cocaine day 4, indicated by yellow column) compared to inhibition of axons from non-activated OFC neurons (gray) (Cre-ON vs. Cre-OFF Day 4: $t(31)=2.08$, $p=0.04$).

(F) CNO infusion into the DS does not influence basal locomotor activity in either group (Cre-ON: paired two-tailed $t(15)= 0.50$, $p=0.62$, Cre-OFF: $t(16)=0.55$, $p=0.59$).

* $p<0.05$.

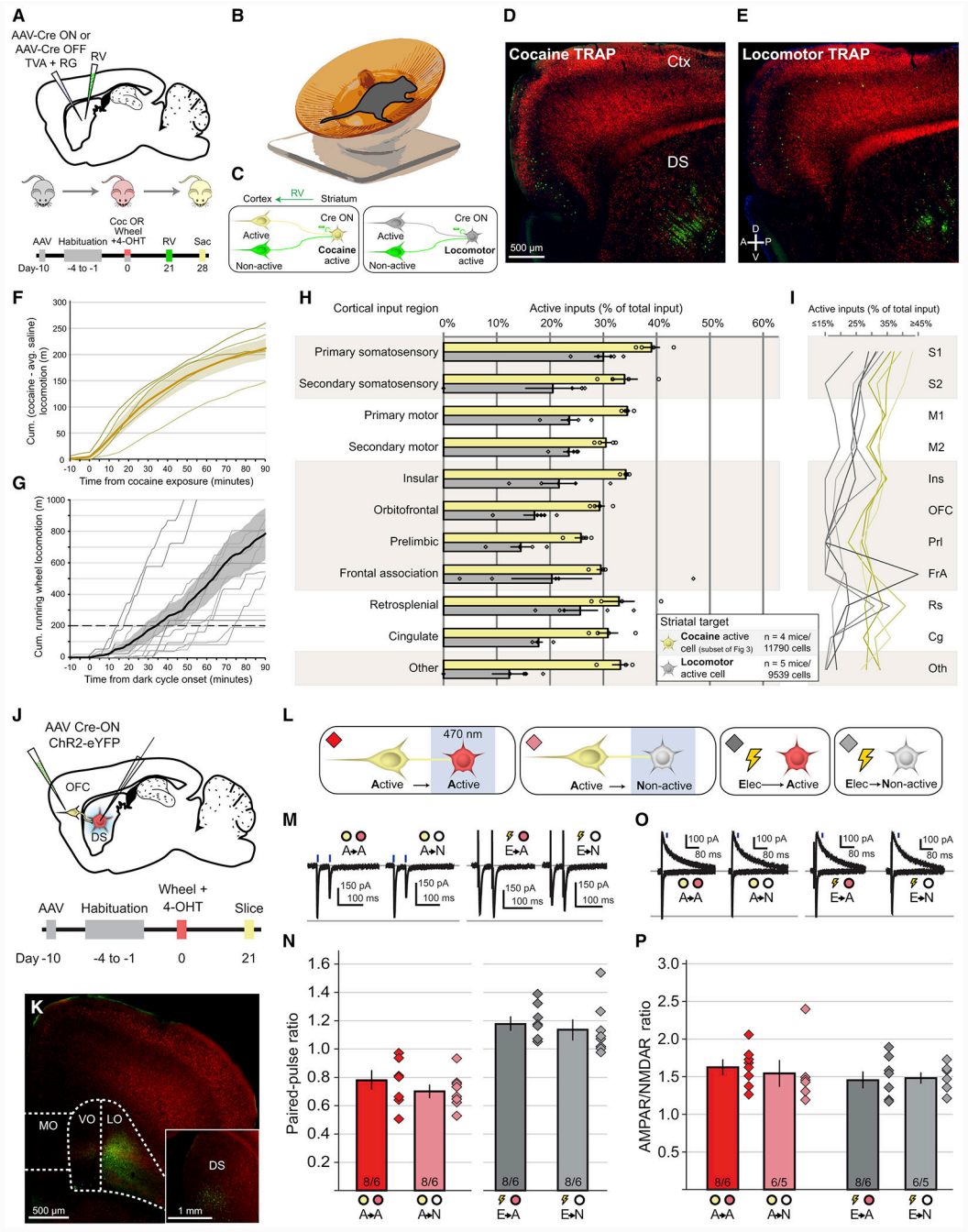

Figure 7. Corticostriatal Neurons Activated by Hyperlocomotion Do Not Show Persistent Enhanced Connectivity with Locomotor-activated Striatal Neurons.

(A) Targeting strategy and timeline for assessing corticostriatal connectivity in either cocaine-exposed animals or hyperlocomotive animals.

(B) Wireless mouse wheel used to assess locomotion in an animal's home cage.

(C) Legend applying to (F-I), where monosynaptic inputs to cocaine-activated DS neurons are labeled yellow, and monosynaptic inputs to locomotor-activated DS neurons are labeled gray.

(D) Viral injection site and cortical retrograde label in a mouse exposed to cocaine. Scale bar applies to (D,E).
(E) Viral injection site and cortical retrograde label in a hyperlocomotive mouse.
(F) Cumulative hyperlocomotion to cocaine exposure. Locomotor activity levels following cocaine injection (n=5 mice) were normalized by subtracting the average activity level of mice injected with saline (n=5 mice). Thin lines indicate individual animals, thick line indicates population mean with shaded bar indicating ± 1 SEM.
(G) Cumulative wheel-based locomotor activity in all mice used in this figure. Dashed line indicates threshold locomotion over 90 minutes necessary for inclusion. Thin lines indicate individual animals, thick line indicates mean with shaded bar indicating ± 1 SEM. Two mice exceeded 1km; these lines are truncated but are included in the population mean.
(H) Proportion of activated cortical input neurons to targeted DS neurons either activated by cocaine (yellow) or by hyperlocomotion (gray). Proportion of active inputs to cocaine-activated cells is different from inputs to locomotor-activated cells (Cocaine vs. Locomotor: Two-way ANOVA: $F(1,77)=85.54$, $p<0.001$). Cohort-matched subset of Cre-ON animals displayed in Figure 3 used for comparison. Each individual data point represents the proportion of active inputs for a single animal. Bars indicate mean ± 1 SEM, and apply to all subsequent panels.
(I) Individual animal data displayed in (H), with each connected line indicating a single animal.
(J) Targeting strategy and timeline for assessing optogenetic assessment of synaptic properties between corticostriatal neurons activated by hyperlocomotion and downstream DS neurons.
(K) Injection site of AAV expressing Cre-ON ChR2 in OFC, with inset of fibers in DS.
(L) Optogenetic activation of axon terminals arising from hyperlocomotion-activated corticostriatal neurons (yellow) while recording from either a hyperlocomotion-activated DS neuron (red) or non-activated neuron (gray). Nonspecific electrical stimulation was also performed while recording from either activated or non-activated neurons. Diamonds color-coded to indicate recording conditions, matched to all subsequent panels.
(M) Representative EPSCs in response to paired-pulse optogenetic activation of hyperlocomotion-activated corticostriatal axons while recording from either hyperlocomotion-activated or non-activated DS neurons. Electrically evoked EPSCs are also plotted.
(N) Paired-pulse ratios for all recording conditions (A→A vs A→N: $t(14)=1.10$, $p=0.29$; E→A vs E→N: $t(14)=0.56$, $p=0.58$).
(O) Representative EPSCs at −70 mV and +50 mV generated by optogenetic or electrical stimulation of corticostriatal axons.
(P) AMPAR/NMDAR ratios for all recording conditions (A→A vs A→N: $t(12)=0.45$, $p=0.66$; E→A vs E→N: $t(12)=0.26$, $p=0.80$).
See also Figure S5.

KEY RESOURCES TABLE

REAGENT or RESOURCE	SOURCE	IDENTIFIER
Bacterial and Virus Strains		
AAV-Cre-ON-TVA: AAV2-CAG-FLEx-TCB	Miyamichi et al., 2013	
AAV-Cre-ON-RG: AAV8-CAG-FLEx-RG	Stanford Gene Vector and Virus Core	GVVC-AAV-59
AAV-Cre-ON-ChR2-eYFP: AAV-DJ-EF1 a-DIO-hChR2(H134R)-eYFP	Stanford Gene Vector and Virus Core	GVVC-AAV-38
AAV-Cre-ON-hM4Di-mCherry: AAV-DJ-EF1 a-DIO-hM4D(Gi)-mCherry	Stanford Gene Vector and Virus Core	GVVC-AAV-129
AAV-Cre-OFF-TVA: AAV2-CAG-FLExOFF-TCB	This paper	
AAV-Cre-OFF-RG: AAV8-CAG-FLExOFF-RG	This paper	
AAV-Cre-OFF-ChR2-eYFP: AAV-DJ-hSyn-FLExOFF-hChR2(H134R)-eYFP	Beier et al., 2017	
AAV-Cre-OFF-hM4Di-mCherry: AAV-DJ-hSyn-FLExOFF-hM4D(Gi)-mCherry	Beier et al., 2017	
(EnvA)RV-ΔG-eGFP	Wickersham et al., 2007	
RV-ΔG-eGFP	Wickersham et al., 2007	
Experimental Models: Cell Lines		
293T-EnvA	Wickersham et al., 2007	
293T-TVA800	Wickersham et al., 2007	
Experimental Models: Organisms/Strains		
Mouse: Arc-TRAP: B6.129(Cg)-Arctm1.1(cre/ERT2)Luo/J	Jackson Laboratory	JAX:021881
Mouse: Ai14: B6.Cg-Gt(ROSA)26Sortm14(CAG-tdTomato)Hze/J	Jackson Laboratory	JAX:007914
Mouse: C57Bl/6J	Jackson Laboratory	JAX:000664
Recombinant DNA		
pAAV-CAG-FLExOFF-TCB	This paper	RRID:Addgene_134980
pAAV-CAG-FLExOFF-RG	This paper	RRID:Addgene_134981
pAAV-hSyn-FLEx-mGFP-2A-Synaptophysin-mRuby	Beier et al., 2015	RRID:Addgene_71760
pAAV-EF1a-double floxed-hChR2(H134R)-eYFP-WPRE-HGHpA	Deisseroth lab	RRID:Addgene_20298
pAAV-hSyn-DIO-hM4D(Gi)-mCherry	Krashes et al., 2011	RRID:Addgene_44362
pAAV-hSyn-FLExOFF-hChR2(H134R)-eYFP	Beier et al., 2017	
pAAV-hSyn-FLExOFF-hM4D(Gi)-mCherry	Beier et al., 2017	
Software and Algorithms		
OriginPro 2018	Origin Labs	RRID:SCR_014212
FIJI	Schindelin et al., 2012	RRID:SCR_002285
Axograph	Axograph	RRID:SCR_014284
OlyVIA	Olympus	
Excel	Microsoft	RRID:SCR_016137
Prism	GraphPad	RRID:SCR_002798